Mask, the *Drosophila* Ankyrin Repeat and KH domain-containing protein, regulates microtubule dynamics

Daniel Martinez[1†], Mingwei Zhu[1†], Jessie J. Guidry[2], Niles Majeste[1], Hui Mao[1], Sarah Yanofsky[1], Xiaolin Tian[1*] and Chunlai Wu[1]

[1]Neuroscience Center of Excellence, Department of Cell Biology and Anatomy, Louisiana State University Health Sciences Center, New Orleans, LA 70112, USA

[2]Proteomics Core Facility, and the Department of Biochemistry and Molecular Biology, Louisiana State University Health Sciences Center, New Orleans, LA 70112, USA

[†] These authors contributed equally

*Corresponding author

LSUHSC-NO, Neuroscience Center of Excellence

2020 Gravier St. STE.D

New Orleans, LA 70112

Phone: 504-568-2007

Email address: xtian@lsuhsc.edu

Author Contribution

D. M. and M.Z. collected and analyzed the majority of the data. M.Z., C.W. and X.T. designed the experiments. J.J.G. and N.M. provided assistance with data analysis, while H.M. and S.Y. provided technical supports. X.T. and C.W. prepared the manuscript.

Abstract

Proper regulation of microtubule (MT) dynamics is vital for essential cellular processes and neuronal activities, including axonal transport as well as synaptic growth and remodeling. Here we demonstrate that Mask negatively regulates MT stability and maintains a balanced dynamics of MT length and architecture in both fly larval muscles and motor neurons. In larval muscles, loss of *mask* increases MT length, and genetically altering *mask* levels modifies the Tau-induced MT fragmentation. In motor neurons, loss of *mask* function reduces the number of End-Binding Protein 1 (EB1)-positive MT plus-end structures in the axons and also results in overexpansion of the presynaptic terminal at larval neuromuscular junctions (NMJs). *mask* shows strong genetic interaction with *stathmin* (*stai*), a neuronal modulator of MT dynamics, in regulation of axon transportation and synaptic terminal stability. Our structure/function analysis on Mask revealed that truncated Mask transgenes carrying only its N-terminal portion that contains the two Ankyrin repeats domains is able to rescue the MT-related *mask* loss-of-function defects in larval muscles and NMJs, suggesting an essential role of the Ankyrin repeats domains in mediating Mask's MT stability-regulating function. Furthermore, we discovered that Mask negatively regulates the abundance of the microtubule-associated protein Jupiter in motor neuron axons, and that neuronal knocking down of *Jupiter* partially suppresses *mask* loss of function phenotypes at the larval NMJs. Together, our study identified Mask as a novel regulator for microtubule stability and dynamics.

Author Summary

Microtubules (MTs) are an essential part of the cellular cytoskeleton, providing the structural basis for critical cellular processes and functionality. A series of factors are required to orchestrate the assembly and disassembly of MTs. Here, we identified Mask as a novel regulator of MT dynamics in *Drosophila*. Mask shows prominent interplay with two important modulators of MT, Tau and Stathmin (Stai). These findings not only support the role of Mask as a novel microtubule regulator but also provide the foundation to explore future therapeutic strategies in mitigating deficits related to dysfunction of Tau and/or Stai, both of which are linked to human neurodegenerative disorders. Further analyses on Mask demonstrated that Jupiter's localization to the MTs in the axons is negatively affected by Mask, and that reducing Jupiter level is able to partially suppress synaptic defects caused by *mask* mutant. Together, these data imply that Mask's function in regulating MT dynamics requires Jupiter.

57 **Introduction**

58 Terminally differentiated postmitotic cells such as neurons and muscles use their microtubule
59 (MT) network not for cell division but rather as architectural components essential for their
60 shape and unique cellular functions. In addition to supporting the structural integrity of the axons
61 and the dynamic morphological changes of the dendritic in neurons, MTs also act as directional
62 railways for transporting materials and organelles between the cell body and the synapses (1).
63 MTs can undergo cycles of dynamic assembly and disassembly (labile state) or stay relatively
64 stable in a cell type- and developmental stage-dependent manner (2). For example, MTs in post-
65 mitotic cells, such as neurons, are generally more stable than MTs in dividing cells. However,
66 within a developing neuron, MTs at the axon growth cone are much more labile than MTs near
67 the soma (3), and even in individual axons, MT network consists of domains that differ in their
68 stability (4). Recent studies suggest that both the stable and labile pools of microtubules play
69 essential roles for normal neuronal function. Furthermore, the spacing among MTs and distance
70 between MT ends have both been shown to be critical for normal axonal transport (5, 6).
71 Therefore, striking a balance in MT dynamic is of vital importance to maintaining MT-mediated
72 cellular functions.

73 Many proteins and pathways have been identified as potential regulators of MT stability
74 (2, 7). Among the major proteins controlling MT stability, Stathmin/SCG10 (superior cervical
75 ganglion-10 protein) and Tau/MAPT are both MT-binding proteins which regulate multiple
76 aspects of MT stability, including growth and shrinkage, as well as the transition between
77 catastrophe and rescue. Both Stathmin and Tau are associated with diverse models of
78 neurodegeneration, axon transport defects, and cancer (8-11). While *in vitro* studies of Stathmin-
79 related proteins in mammals suggest that Stathmin promotes destabilization of MTs, studies of

80 *stathmin* (*stai*) in fly neuromuscular junction (NMJs) showed that it is required for MT
81 stabilization, as well as axon transport and NMJ stability (12, 13). The results of the *in vivo*
82 studies in mammals is consistent with the fly data in that *stathmin* knockout mice exhibit age-
83 dependent axonopathy in both the central and peripheral nervous systems, and they exhibit
84 defective motor axon outgrowth and regeneration (14, 15). Tau, on the other hand, plays a
85 multifaceted role in cell survival signaling. Loss of Tau function or high levels of
86 hyperphosphorylated Tau disrupts MT stability, leading to axonal transportation defects in motor
87 neurons and microtubule breakdown in larval muscles (16). Additionally, hyperphosphorylated
88 Tau aggregates form inclusion bodies that are associated with a variety of disorders collectively
89 referred to as tauopathies, including Alzheimer's disease(17). In animal models, such as rodents
90 and fruit flies, overexpression of human Tau in the neuronal tissues leads to progressive
91 neurodegeneration (18).

92 Mask is a 4001-amino-acid protein with several functional domains. It consists of two
93 Ankyrin Repeats, one Nuclear Export Signal (NES), one Nuclear Localization Signal (NLS), and
94 a C-terminal KH domain. The two Ankyrin repeat domains containing 15 and 10 tandem
95 Ankyrin repeats likely coordinately facilitate the ability of Mask to associate with other proteins,
96 according to the well-documented involvement of the Ankyrin domains in mediating protein-
97 protein interactions in eukaryotic cells (19). The NES and NLS motifs may be required for
98 shuttling Mask protein in and out of the nucleus, which is essential for its interaction with the
99 Hippo pathway effector Yorkie/YAP in mitotic cells (20, 21). The KH domain is an
100 evolutionarily conserved motif that is about 70 amino acids long, and it was first identified in the
101 human heterogeneous nuclear ribonucleoprotein K (22). KH domains bind RNA or single-
102 stranded DNA (ssDNA) and are found in proteins involved in transcription, translation and

103 mRNA stability regulation (23, 24). Mask has been linked to several signaling pathways and
104 different cellular processes in mitotic cells- it regulates cell proliferation during development
105 (25); it is a component of the centrosome and nuclear matrix (26, 27) and a co-transcription
106 factor of the Hippo pathway (20, 21). The human homolog of Mask, ANKHD1, is expressed at
107 relatively high levels in acute leukemia cells (28), multiple myeloma cells (29) and prostate
108 cancer cells (30). In the cancer cells, ANKHD1 is shown to be able to suppress p21 (31) and
109 Stathmin activity (32). Regardless the attentions that has been casted on its function in mitotic
110 cells, the functions of Mask and its vertebrate homolog in post-mitotic cells, including neurons
111 and muscle cells, is largely unknown. Our previous studies on Mask demonstrated that Mask
112 regulates mitochondrial morphology (33) and promotes autophagy (34) in larval muscles. Here,
113 we show that Mask is required for balanced MT stability in muscle and neurons, two post-mitotic
114 cell types, and that Mask genetically interacts with two MT-interacting proteins, Tau and
115 Stathmin, whose dysfunctions are linked with human diseases. Furthermore, the abundance of
116 Jupiter, a microtubule-associated protein, is reversely related to Mask levels in the motor neuron
117 axons. Knocking down *Jupiter* in the neurons partially suppresses the morphological defects
118 caused by *mask* loss-of-function at the larval NMJs. Together, our studies demonstrated a novel
119 function of Mask in regulating microtubule dynamics.

120 **Results**

121 Mask negatively regulates MT length in larval muscles

122 Our previous studies of the putative scaffolding protein Mask demonstrated that overexpressing
123 Mask ameliorate the degeneration of photoreceptors caused by overexpressing Tau in adult fly
124 eyes (34). This finding prompted us to explore further potential interplays between Mask and
125 Tau in the context of microtubule (MT) morphology, given the fact that Tau is a well-studied
126 MT-binding protein. We first examined MT morphology in *mask* loss-of-function mutants.
127 Interestingly, we found that, in the larval body wall muscles, the MTs in the *mask* null mutants
128 are substantially longer than those in the wild type control, particularly in the area surrounding
129 the muscle nuclei (Fig. 1AB). Such a phenotype is fully rescued by introducing the UAS-Mask
130 transgene back to the *mask* mutant larval muscles (Fig. 1AB). To further confirm this finding, we
131 introduced UAS-*mask* RNAi to the wild type larval muscle and found that *mask* knockdown also
132 moderately increased muscular MT length (Fig. 1AB). These data suggested that one of the
133 normal functions of Mask in larval muscles is to restrain MT length.

134 Loss of *mask* function suppresses, while upregulation of Mask enhances Tau-induced MT
135 breakdown and toxicity in fly muscles

136 Next, we examined the interplay between Mask and Tau in regulating the MT network in larval
137 muscles. Overexpression of human Tau together with UAS-tdTomato (control) in fly muscles
138 causes severe destruction of the MT network, and the affected MTs becomes short and punctate
139 (Fig. 1 C), which is consistent with a previously reported study on human Tau overexpression in
140 fly muscles (16). *mask* RNAi in the muscle, with its effects to increase MT length, was able to
141 substantially reverse the shortened MT length caused by Tau-overexpression. Overexpressing

142 Mask alone in wild type muscles, on the other hand, although alone does not lead to obvious
143 reduction in the MT length in larval body wall muscles (Fig. 1AB), when co-expressed with Tau
144 further devastates the MT network – MT almost only exists in bright rod-shaped puncta (Fig.
145 1C,D), suggesting the ability of Mask-overexpression to impact MT morphology under the
146 sensitized background. To test whether Mask knockdown or overexpression alter the expression
147 levels of human Tau, which in turn modifies Tau-induced MT defects, we examined the
148 expression levels of human Tau under the conditions of up- or down-regulation of Mask.
149 Expression of human Tau in the muscles is increased when it is co-expressed with UAS-Mask
150 RNAi, suggested that the suppression effects are not induced by reducing Tau expression level
151 by Mask knockdown (Fig. S1). Similarly, levels of human Tau expression in the muscle are
152 decreased when it is co-expressed with UAS-Mask, therefore, the enhancement of the MT
153 fragmentation is not a result of further elevation of Tau in the muscles (Fig. S1). These data are
154 consistent with our previous finding that Mask actively promotes autophagy and degradation of
155 aggregation-prone proteins in larval muscles (34).

156 Our morphological and genetic analyses suggested that the normal function of *mask* is to restrain
157 MT length. To further confirm this notion, we used additional biochemical analysis to examine
158 the overall distribution of MT length in the cell lysates of wild type or *mask* knockdown larval
159 muscles. We found that reducing Mask levels does not alter the total Tubulin concentration in
160 muscle homogenates (Fig. 2A). In the presence of 100 μM taxol (a potent concentration that
161 promotes microtubule polymerization), Tubulin proteins in both control and mask *knockdown*
162 lysates polymerize and fractionate exclusively in the pellet after ultracentrifugation (Fig. 2A). In
163 the presence of 0.1 μM taxol (a concentration that reverses a steady state of MT dynamic status),
164 *mask* RNAi lysate contains more Tubulin proteins that fractionate with pellet fraction (Fig. 2 A,

165 B) compared to the control condition, suggesting that loss of Mask activity in muscles results in
166 a MT network that is comprised of longer MTs.

167 Mask regulates presynaptic terminal growth in neuromuscular junctions

168 The prominent protective effects of Mask in the photoreceptors (35) also prompted us to
169 analyzed the neuronal functions of *mask* using the fly larval NMJ as a model synapse. We found
170 that *mask* null mutant ($mask^{10.22/Df}$) NMJs show expanded presynaptic terminal growth reflected
171 by an increased number of bouton, synaptic span, and number of branching points (Fig. 3AB).
172 Such a morphological defect is due to loss-of-function of *mask* in the presynaptic motor neurons
173 as pan-neuronal or ubiquitous expression, but not muscle (postsynaptic) expression, of UAS-
174 Mask rescues the NMJ overgrowth phenotype in *mask* null mutants (Fig. 3AB). Furthermore,
175 neuronal knockdown of *mask* using a UAS-*mask* RNAi causes similar NMJ expansion as *mask*
176 mutants (Fig. 3AB). These data demonstrate that Mask regulates normal NMJ expansion in a
177 cell-autonomous manner in neurons. Given that microtubule stability has a direct impact on
178 synaptic size and morphology(36), we then investigated whether the neuronal regulation on the
179 presynaptic expansion by Mask is connected with its function in regulating MT dynamics. We
180 first analyzed MT dynamics in the segmental nerve using the MT plus-end tracking protein End-
181 Binding Protein 1 (EB1) (37) as the marker to assess the abundance of the MT plus-end
182 structures. In motor neuron axons, EB1-GFP proteins exhibit two types of localization patterns -
183 a uniform distribution along the axons, and bright comets scattered within the axons- the signals
184 that represent the accumulation of the end-binding protein at the MT plus-ends. We found that
185 the numbers of the EB1-GFP comets are significantly reduced by neuronal knockdown of *mask*
186 when compared to the controls (Fig. 3CD). These results together suggest that loss of *mask* leads

187 to formation of fewer plus-end structures, and that MTs present in the axons are likely
188 structurally longer and less dynamic.

189 *mask* and *stathmin* genetically interact with each other to regulate morphology and structural
190 stability of NMJs.

191 To further investigate Mask's action in regulating MT elongation in neurons, we tested genetic
192 interaction between *mask* and *stathmin. stathmin* is a well-established modulator of MT stability
193 in neurons. Loss of *stathmin* causes severe destabilization of MT in motor neurons, resulting in
194 axonal transport defects, especially in the posterior segments, as well as premature loss of
195 presynaptic structure at the nerve terminals (named the "footprint" phenotype in *Drosophila*
196 neuromuscular junctions) (12, 13). Mammalian studies showed that ANKHD1, the human
197 homolog of *mask*, regulates the activity of Stathmin 1 in leukemia cells(32), suggesting a
198 possible link between the two genes in neurons. We found that the presynaptic NMJ expansion
199 observed in *mask* mutant NMJs is completely suppressed in the *stai/mask* double mutant NMJs
200 (Fig. 3AB). Similarly, the NMJ expansion phenotype induced by neuronal knockdown (RNAi)
201 of *mask* can also be partially suppressed by a heterozygous *stai* mutant, and completely
202 suppressed by the homozygous *stai* mutant (Fig. 4AB), suggesting a strong genetic interaction
203 between the two genes. In addition, *mask* loss of function can also reversely suppress neuronal
204 defects caused by loss of function of *stai*. Both the footprint phenotype and the axonal transport
205 defect of *stai* mutants are partially suppressed by the neuronal knockdown of *mask*, and
206 completely suppressed by the *mask* null mutant (Fig. 4CD), suggesting that the enhanced MT
207 stability by *mask* loss of function is able to compensate the impaired MT stability caused by loss
208 of *stai*. These data provides strong evidences to support the notion that *mask* and *stai* exert

209 opposite effects on MTs and these effects antagonize each other in regard to MT stability. The
210 strong genetic interactions between *mask* and *stai* further suggest that *mask* regulates synaptic
211 morphology and formation at the larval NMJs via its control over MT stability.

212 Structure and function analysis of Mask for its action in modulating MT stability

213 The inclusion of numerous functional domains/motifs in Mask suggests a structural division for
214 its diverse functions. In order to determine the domain(s) requirement for the different functions
215 of Mask, we generated UAS-Mask transgenes that carry a GRGG to GDDG mutation in their KH
216 domain (named UAS-Mask-KH-Mut). Recent studies showed that mutating the GXXG loop to
217 GDDG in the KH minimal motif reduced the ability of the KH domain to bind RNAs (38). The
218 GXXG loop of Mask resides in amino acid 3053-3056 as GRGG, which is completely conserved
219 between fly Mask and human ANKHD1 (corresponding sequence 1710-1713). We also
220 generated UAS-Mask deletion transgenes that lack either N- or C-terminal portions of the protein
221 (depicted in Fig. 5A). One resulting transgene contains the N-terminal two Ankyrin repeats
222 clusters (named Mask-ANK), and the other resulting transgene lacks the N-terminal portion of
223 Mask but contains the NES, NLS, and KH domains (named Mask-KH-Only).

224 We next expressed the mutant *mask* transgenes in the larval muscles in the *mask* null
225 mutants and confirmed that all transgenes express with the predicted molecular weight (Fig. 5A).
226 We then tested the functionality of these transgenes by examining their abilities to rescue the
227 MT-related *mask* mutant defects in larval muscles and NMJs rescue the loss of function
228 phenotypes of Mask in larval muscles and neurons. We found that the UAS-Mask-KH-Mut
229 transgene rescues the MT phenotype in muscles (Fig. 5BC) as well as the defects of NMJ
230 expansion at the NMJs in *mask* mutants (Fig. 5DE) to a level that is comparable to wild type

231 UAS-Mask transgene. These results suggest that the function of the KH domain is not required
232 for the activity of Mask in regulating MT stability or presynaptic terminal expansion.
233 Meanwhile, the UAS-Mask-ANK, but not the UAS-Mask-KH-Only transgene, also rescues the
234 muscle MT length and NMJ overexpansion phenotypes in *mask* mutant larvae (Fig. 5B-E).
235 Together, these data suggest that the N-terminal portion of the Mask protein that contains the
236 Ankyrin repeats domains is sufficient to mediate Mask's action in regulating MT stability, while
237 the NES, NLS and KH domain are dispensable for the MT-regulating function of Mask.

238 Mask inhibits the abundance of the MA-associated protein Jupiter in the axons

239 To further understand *mask*-mediated regulation of MT stability, we analyzed the
240 distribution and abundance of two MT-associated proteins Jupiter and Futsch proteins in the
241 motor neurons, two other proteins that have been implicated in the stabilization of MT (39, 40).
242 When expressed in the neurons, the Jupiter-mCherry transgene is detected primarily on the axons
243 with low degree extension into the nerve terminals in the area that immediately connects axons
244 and synapses, and these patterns change in response to Mask. The intensity of Jupiter-mCherry in
245 the segmental nerves is substantially enhanced by *mask* loss-of-function, while reduced by Mask
246 overexpression (Fig. 6AB). In addition, the increased abundance of mCherry-Jupiter caused by
247 *mask* RNAi also leads to the extension of mCherry-Jupiter into the nerve terminal; while the
248 reduced mCherry-Jupiter abundance caused by Mask overexpression leads to retraction of
249 mCherry-Jupiter further away from the nerve terminals. To test whether changes of Jupiter-
250 mCherry total protein levels underlie its altered abundances on the MTs, we measured the
251 protein levels of mCherry-Jupiter in larval brain lysates. Neither *mask* RNAi nor overexpression
252 changed the proteins levels of mCherry-Jupiter (Fig. S2A), suggesting that Mask specifically
253 regulates Jupiter's MT localization which reflects status of MT stability and dynamic. In contrast

254 to Jupiter, we detected no significant changes in Futsch intensity or distribution in segmental
255 nerves or NMJs in response to up- or down-regulation of Mask levels (Fig. 6A-D). Together,
256 these data suggest that Mask negatively regulates the MT localization of MT-associated protein
257 Jupiter. It is worth noting that Jupiter-mCherry and Futsch appear to preferentially label distinct
258 pools of MTs within the axons, which is more prominent in the segmental nerves of Mask-
259 knockdown animals (Fig. S2B). Although there is no precedent evidence supporting the
260 existence of distinct Jupiter-positive and Futsch-positive MT species that may be structurally and
261 functionally different from one another, our data supports the notion that Mask inhibits the
262 decoration of MTs by mCherry-Jupiter but not Futsch.

263 Given the molecular regulation of Jupiter by Mask, we next test the functional
264 connections between *jupiter* and *mask* by analyzing the genetic interactions between the two
265 genes. First, we found that overexpressing Jupiter-mCherry in neurons enhances the lethality
266 caused by null mutations of *mask*- *mask* mutant larvae die at late larval stage; while
267 overexpressing Jupiter in the *mask* null mutant induces lethality at embryonic stage. 26.1% of the
268 progenies (n = 226) from the cross between $mask^{10.22}/TM6B$ and $mask^{Df317}/TM6B$ are non-Tubby
269 larvae ($mask^{10.22/Df317}$), and these progenies can survive up to the 3rd instar larval stage. However,
270 no non-Tubby larvae can be found in the progenies (n = 523) when Jupiter is overexpressed in
271 the *mask* mutants. Second, knocking down *Jupiter* in neurons can partially suppress the
272 morphological defects caused by *mask* loss of function at the larval NMJs. A *Jupiter* RNAi line
273 that can efficiently knock down *Jupiter* transcript levels to ~33% of wild type level in neurons
274 (Fig. S3AB), when expressed in *mask* null mutant, can significantly suppress the increased
275 synaptic span and branching point phenotypes (Fig. 6EF) with increased bouton number
276 phenotype in *mask* mutant NMJs unaffected. Together, these strong genetic interactions between

277 *jupiter* and *mask* not only provide a functional link between the two genes but also further
278 support a model where Jupiter works downstream of Mask in regulating MT stability, and that
279 Mask regulates MT dynamics via directly or indirectly inhibiting the MT localization of Jupiter.
280 Furthermore, although Jupiter RNAi does not cause defects in synaptic growth by itself, its
281 genetic interactions with Mask provide new evidence to support the function of Jupiter to
282 stabilize MT.

283 **Discussion**

284 The characteristics of MT organization and dynamics are cell-type specific. In non-neuronal
285 cells, MTs are labile and undergo frequent growth and shrinkage due to dynamic instability (41).
286 In neurons, MTs are generally more stable than MTs in the dividing cells, however recent studies
287 indicate that there are also abundant labile MT fraction in neurons, especially in the developing
288 neurons, and that a balance between labile and stable MT fractions contribute to normal neuronal
289 functions (4). A key MT-mediated neuronal function is axonal transport. Recent *in vivo* imaging
290 studies of *C. elegans* motor neurons showed that the tiling of the MT fragments in axons is
291 tightly regulated, and such intrinsic MT organization provides the structural basis for efficient
292 cargo transportation along the axons (6).

293 Decades of studies have demonstrated that MT dynamics are tightly regulated by a
294 number of mechanisms including GTP/GDP ratio, post-translational modification of MT, as well
295 as a vast array of MT-stabilizing, MT polymerizing and depolymerizing, and MT-severing
296 proteins. Our studies identify Mask as a novel regulator of MT stability that controls normal
297 neuronal morphology during development and modulates MT dynamics in concert with factors
298 such as *stai* and Tau that are related to human neuronal pathological conditions. Loss of *mask*

299 resulted in elongated MTs in larval muscles as well as presynaptic over-expansion at the fly
300 larval NMJs, a possible consequence of the over-stabilization of MT given that this phenotype is
301 strongly suppressed by *stai*-induced MT destabilization and partially suppressed by Jupiter
302 knockdown in neurons.

303 The involvement of Mask in regulating MT stability is further supported by its genetic
304 interactions with *stathmin* and Tau. Previous studies on the effects of overexpressing human Tau
305 protein in fly muscles showed that these ectopic Tau proteins are hyperphosphorylated and cause
306 reduced MT density and enhanced fragmentation, similar to the finding in AD patients and
307 mouse models (16). We found that Mask is able to modulate the Tau-induced MT fragmentation.
308 Loss of Mask enhances, while gain of Mask suppresses MT fragmentation caused by Tau.
309 Neuronal Stathmin family proteins are regulators of MT stability, and perturbation of Stathmin
310 expression impacts neuronal development, plasticity, and regeneration (42). *Drosophila stathmin*
311 mutations cause severely disrupted axonal transport and presynaptic nerve terminal stabilization
312 at the larval NMJs, likely due to impaired integrity of the MT network (12, 13). Knocking out
313 mammalian STMN2, also known as SCG10, results in defects in axon outgrowth and
314 regeneration (15). The result that loss of *mask* in neurons suppresses *stai*-induced axon transport
315 and NMJ development phenotype in a dose-dependent manner, suggesting that Mask antagonizes
316 the action of Stathmin in regulating MT stability. These data also suggested that there is a
317 potential that disturbed dynamics of the MT network under certain pathological conditions can
318 be restored by manipulating Mask levels.

319 We previously reported that Mask regulates autophagy in fly larval muscles (34). In line
320 with the function of Mask, the levels of ectopic human Tau protein were significantly reduced

321 when co-expressed with Mask, and it is substantially increased when co-expressed with *mask*
322 RNAi (Fig. S1). In addition, Tau proteins in *mask*-knockdown muscles start to form aggregated
323 puncta, possibly due to the excessively elevated levels of the Tau protein. Overexpressing Tau in
324 the muscles causes the developing animals to die at the pupal stages but simultaneously knocking
325 down *mask* suppresses this lethality (unpublished). These findings are very interesting as they
326 demonstrates that the formation of the Tau aggregates does not directly correlate with the
327 toxicity and lethality caused by Tau overexpression in the muscles. It is mostly likely that the
328 toxicity is primarily caused by the severe MT fragmentation induced by Tau expression. MT
329 fragmentation induced by Tau does not seem to be correlative to Tau protein levels, as co-
330 overexpressing Mask with Tau not only significantly reduces the levels of the exogenously
331 expressed Tau protein (Fig. S1) but also potently enhances MT fragmentation (Fig. 1). Although
332 these findings are not directly linked to this study on Mask, they suggest that dysregulation on
333 Tau may cause defects in MT organization that is independent to the toxicity induced by Tau
334 aggregates.

335 Our loss-of-function studies demonstrated that *mask* is required for normal MT
336 organization in both neurons and muscles. However, overexpression of Mask reduces MT length
337 only under a sensitized background where human Tau induces severe MT fragmentation, but not
338 under an otherwise wild type background, indicating that Mask overexpression itself does not
339 drive significant change in MT dynamics. Mask is a large scaffolding protein containing two
340 ankyrin repeats at its N-terminal and a KH-domain at its C-terminal. Ankyrin-repeats-containing
341 proteins have been implicated in the regulation of MT dynamics. Two isoforms of *Drosophila*
342 Ankyrin2, Ank2-L and Ank2-XL, regulate MT spacing in conjunction with Futsch, and are
343 involved with control of both axon caliber and transport (43). The KH-domain, on the other

344 hand, may mediate Mask's action in regulating RNA alternative splicing (44) as well as
345 transcription through the HIPPO pathway (20, 21). Our structure/function studies of Mask's
346 functional domains suggested that the two Ankyrin repeats domains, but not the KH domain, of
347 Mask are essential for Mask's ability to negatively regulate MT dynamics. The data demonstrate
348 that the Mask transgene containing the N-terminal two Ankyrin repeats domains rescues the MT
349 length in *mask* mutant larval muscles to a level similar to the wild type Mask transgene.
350 Moreover, when expressed in neurons, the same MASK-ANK transgene can also potently
351 rescues synaptic terminal overexpansion in *mask* mutant NMJs, providing not only knowledge
352 for the structural basis of Mask-mediated regulation of MTs but also additional evidence of MT-
353 dependent synaptic regulation by Mask. The sufficiency of Mask's Ankyrin-repeats domains and
354 the disposableness of the KH domain for MT-regulating function of Mask suggests that protein-
355 protein interactions, but not directly binding to RNAs or DNAs are essential for Mask to regulate
356 MT dynamics. It is interesting that while the KH domain may not be essential for Mask's action
357 in regulating MT stability, it is required for Mask's activity in promoting autophagy. The KH
358 domain mutation that diminishes its RNA-binding capacity largely abolishes Mask's ability to
359 elevate autophagic flux in larval muscles (unpublished data). These results indicate that different
360 functions of Mask are structurally separable and could be modulated independently. Future
361 studies that further investigate the related molecular details will help us to understand how
362 diverse functions of Mask are regulated.

363 Studies at the fly larval neuromuscular junction have demonstrated complexed
364 mechanisms regulating presynaptic development. A number of evolutionarily conserved
365 pathways, such as the RPM-1/Hiw/Phr1-mediated ubiquitin pathways (45), the BMP signaling
366 pathway (46, 47) and the Wnt signaling pathway (48) are shown to control the normal

367 presynaptic terminal size. Microtubule cytoskeleton also plays essential roles to sustain synaptic
368 morphology and function. Factors that directly regulate microtubule stability have been shown to
369 impact axon transportation or synaptic structures. For example, Stathmin (12, 13), Ringer and
370 Futsch (40), and dTACC (transforming acidic coiled coil) (36) regulate synaptic terminal growth
371 at the fly NMJs, providing direct evidence supporting a link between MT network dynamics and
372 the presynaptic size and morphology. Some signaling pathways control synaptic growth by
373 targeting MT stability, such as the *wg* signaling (49) and the FoxO pathway (50). Our data
374 demonstrate that loss of *mask* function stabilizes MT and promotes presynaptic expansion,
375 providing additional evidence for a strong association between MT stability and synaptic size.
376 Although we don't have evidence to link Mask to the known signaling pathways that control
377 synaptic growth of the larval NMJs, our imaging and genetic analyses of *mask* loss-of-function
378 phenotypes suggest that Mask negatively regulates MT stability by inhibiting the abundance of
379 Jupiter-associated, but not Futsch-associated MTs. Jupiter is an known microtubule-associated
380 proteins, and has been widely used as a marker for stabilized MTs(39, 51). It's been speculated
381 that Jupiter promotes MT stabilization, although direct evidence is lacking. Our analysis on
382 Mask and Jupiter here provides additional evidence to support a MT stabilizer function for
383 Jupiter. It is unclear how Mask inhibits MT localization of Jupiter, directly or indirectly, at what
384 cellular compartment, and during what stage of cellular differentiation does this inhibition take
385 place. Mask is a protein that is distributed uniformly in the cytoplasm{Smith, 2002 #737}{Zhu,
386 2015 #736}, while Jupiter is a MT-associated protein that also shows dynamic localization in
387 embryonic dividing cells{Karpova, 2006 #993}. Could these two proteins interact transiently
388 which impacts the ability of Jupiter to localize to the MTs, or alternatively, Mask may affect
389 properties of MTs which then consequentially prevent Jupiter from binding to MTs? Moreover,

390 Mask may also act at different stages to regulate MT morphology. The result that *mask* genetic
391 null mutants and *mask* RNAi cause MT defects in larval muscles with different severities-the
392 genetic mutants that abolishes Mask functions early and causes more severe phenotypes, while
393 muscle RNAi only diminishes Mask levels at later stage causes milder defects, suggests that
394 Mask regulates MT stability and dynamics at different stages of MT network formation.
395 Although our result suggests that Mask regulates MT through inhibiting MT localization of
396 Jupiter, the result that knocking down Jupiter can only partially suppress *mask* loss of function
397 phenotypes suggests that Jupiter may not be the only downstream effectors of Mask, and other
398 factors may exist to work together with Jupiter to mediate Mask's effects on MT dynamics. Do
399 these factors actually exist and if yes, what are their molecular identities? All these questions
400 await further investigations.

401 **Materials and Methods**

402 *Drosophila strains, transgenes and genetics*

403 Flies were maintained at 25°C on standard food. The following strains were used in this study:
404 $mask^{10.22}$ (25), $mask^{Df317}$, UAS-Jupiter-mCherry (52), BG380-Gal4 (neuron-specific) (53), Elav-
405 Gal4 (neuron-specific), MHC-Gal4 (muscle-specific), 24B-GAL4 (muscle-specific), DA-Gal4
406 (Ubiquitous), UAS-control-RNAi (P{TRiP.JF01147}), UAS-*mask*-RNAi (P{TRiP.HMS01045})
407 from the Bloomington stock center; UAS-*Jupiter*-RNAi (KK116151) from VDRC. Generation
408 of the full-length wild type *mask* cDNA was previously described (33). This cDNA was used to
409 generate mutant and truncated *mask* cDNA, including pUAST-Mask-KH, pUAST-GFP-Mask-
410 KH-Only, pUAST-Mask-Ank. To generate the UAS-Mask-KH-Mut transgenes, a
411 complementary primer pair containing the mutated coding sequence (GGAGACGATGGA,

412 mutations underlined) were used to facilitate the change the amino acid sequence (AA3053-
413 3056) from GRGG in the wild type Mask to GDDG in the Mask-KH-Mut transgene. We used
414 the QuickChange II XL site-mutagenesis kit (from Agilent Technology, Santa Clara, CA) to
415 substitute wild type sequence with the mutant sequence. The entire UAS-Mask-KH-Mut coding
416 region was then sequenced to ensure no unintended mutations were introduced. To generate the
417 UAS-Mask-ANK and UAS-Mask-KH-Only transgenes, the KpnI (8001) site was used to
418 separate the Mask encoding region into an N- and a C-terminal fragment, each was then used to
419 generate the pUAST-Mask-ANK and pUAST-Mask-KH-Only respectively. All transgenic fly
420 lines were generated by BestGene Inc. (Chino Hills, CA, USA).

421 *Western blots*

422 Western blots were performed according to standard procedures. The following primary
423 antibodies were used: mouse anti-β-Tubulin (1:1,000, E7) mouse anti-Alpha-Actin (1:1000,
424 JLA20) from Developmental Studies Hybridoma Bank; rabbit anti-Mask (1:2,000) (25), mouse
425 anti-mCherry antibody (1:1000, 1C51, NBP1-96752 Novus Biologicals), and rabbit anti-GFP
426 (1:1000, A11122, Invitrogen). All secondary antibodies were used at 1:10,000. Data were
427 collected using Luminescent Image Analyzer LAS-3000 (FUJIFILM) and quantified using Multi
428 Gauge (FUJIFILM).

429 *Immunocytochemistry*

430 Third instar larvae were dissected in ice-cold PBS and fixed in 4% PFA for 30 min. The fixed
431 tissues were stained following standard procedures. The primary antibodies used were: mouse
432 anti-DLG, anti-Futsch and anti-β-Tubulin antibodies from Developmental Studies Hybridoma
433 Bank; rabbit anti-DVGlut (54), rabbit anti-GFP (A11122, Invitrogen) at 1:1000, rabbit anti-

434 mCherry (632496, Clontech) at 1:1000, mouse anti-Acetylated Tubulin (T6793, Sigma) 1:1,000,
435 mouse anti-Tau (12-6400, Invitrogen) at 1: 1000, Cy3-conjugated goat anti-HRP, and Cy5-
436 conjugated goat anti-HRP. The following secondary antibodies (from Jackson
437 ImmunoResearch) were used: Cy3-conjugated goat anti-rabbit IgG at 1:1000, Dylight-488-
438 conjugated anti-mouse IgG at 1:1000, and Alexa-Fluor-647-conjugated goat anti-HRP at 1:1000.

439 *Confocal imaging and analysis*

440 Single-layer or z-stack confocal images were captured on a Nikon (Tokyo, Japan) C1 confocal
441 microscope. Images shown in the same figure were acquired using the same gain from samples
442 that had been simultaneously fixed and stained. For quantification of microtubule length, z-stack
443 confocal images of microtubule in larval muscle 6/7 in segment A2 were obtained double-
444 blinded, and IMARIS software (Bitplane, Inc) was used to quantify average MT length in
445 randomly-selected muscle areas (see below for details).

446 The number of boutons and branching points on larval muscle 4 of segments A2-A4 were
447 manually counted. Measurements of synaptic span (total length of NMJs on the muscle surface)
448 as well as the bouton and branching point counts on the same muscle 4 were performed using
449 NIS-Elements (Nikon) imaging software. The synaptic expansions were measured using Nikon
450 elements manual measurement tools. Muscle areas of each corresponding muscle 4 were
451 measured using an eyepiece reticle—a crossline micrometer ruler— under a 20X objective, and
452 the muscle area was used to normalize all three NMJ parameters.

453 The ration of the nerve terminal distribution of Jupiter-mCherry at the NMJs was measured as
454 the ration of the length of detectable Jupiter-mCherry signal in the nerve terminal to the total
455 length of the same nerve terminal analyzed.

456 *Quantification of microtubule length in fly larval muscles*

457 Microtubule length was analyzed using IMARIS 9.2.1 imaging software. The analysis was
458 performed in a double-blinded manner. An 80 µm × 80 µm (1024×1024 pixel resolution) confocal
459 image for muscle 6 was used in the analysis, and a vertical step size of 0.15 µm was utilized in
460 order to precisely capture the entire depth of muscle volume containing the microtubule network.
461 From each image, two 30 × 30 µm areas of reasonable clarity were selected for quantification. For
462 each randomly chosen area, 100 +/− 50 tracings were performed manually (assisted by IMARIS),
463 with the total number of traces for each muscle sample averaging ~250 filaments. In order to
464 ensure accurate microtubule tracing and end-to-end length measurements in three-dimensional
465 space, it was necessary to regularly switch between the 3D and layer-by-layer views of the imaged
466 microtubule mesh. Additionally, the angle of the confocal image's perspective was often changed
467 to allow for further confirmation that a single microtubule filament was being traced.

468 *Fractionation of Tubulin*

469 Fractionation of β-tubulin was performed as described by Xiong *et al.* with minor modifications
470 (16). Larval muscles of 20 larvae from each genotype were dissected in PBS at room temperature
471 (RT). These muscles were immediately homogenized in 300 ul lysis buffer (150mM KCl, 2mM
472 $MgCl_2$, 50mM Tris, pH 7.5, 2mM EGTA, 2% glycerol, 0.125% Triton X-100, protease inhibitor
473 cocktail) containing either 100 µM or 100 nM Taxol. After incubating for 10 min at RT, the
474 homogenates were centrifuged at 1,500 X g for 5 minutes at RT to remove cellular debris. A
475 small aliquot of the supernatant of each sample was collected to analyze the total β-Tubulin
476 level. The remaining supernatant was ultra-centrifuged at 100,000 g for 30 minutes. After

477 ultracentrifugation, each supernatant and pellet were separated and analyzed by SDS-PAGE and
478 western blots.

479 *Statistical analysis*

480 Statistical analysis was performed, and graphs were generated in Origin (Origin Lab,
481 Northampton, MA). Each data set was normalized and then compared with other samples in the
482 group (more than two) using ANOVA followed by post-hoc analysis with Turkey's test, or with
483 the other sample in a group of two using T-test. All histograms are shown as mean ± SEM. The n
484 numbers of each statistical analysis are indicated in each graph.

Acknowledgments

We would like to thank Michael Simon for the *mask* mutant alleles and the anti-Mask antibodies, Chris Doe for the UAS-Jupiter-mCherry transgene, the VDRC and the Bloomington Stock center for other fly stocks, and Developmental Studies Hybridoma Bank, created by the NICHD of the NIH and maintained at The University of Iowa, Department of Biology, Iowa City, IA 52242, for antibodies. We also thank Liz McGehee for editorial assistance. This work is supported by a Start-up fund from LSUHSC to X.T. and an ALS Association Grant (18-IIA-414) to C.W.

493 **References**

494 1. Kapitein LC, Hoogenraad CC. Building the Neuronal Microtubule Cytoskeleton. Neuron.
495 2015;87(3):492-506.
496 2. van der Vaart B, Akhmanova A, Straube A. Regulation of microtubule dynamic instability.
497 Biochem Soc Trans. 2009;37(Pt 5):1007-13.
498 3. Hur EM, Saijilafu, Zhou FQ. Growing the growth cone: remodeling the cytoskeleton to promote
499 axon regeneration. Trends Neurosci. 2012;35(3):164-74.
500 4. Baas PW, Rao AN, Matamoros AJ, Leo L. Stability properties of neuronal microtubules.
501 Cytoskeleton (Hoboken, NJ). 2016;73(9):442-60.
502 5. Hahn I, Voelzmann A, Liew Y-T, Costa-Gomes B, Prokop A. The model of local axon homeostasis -
503 explaining the role and regulation of microtubule bundles in axon maintenance and pathology. Neural
504 Development. 2019;14(1):11.
505 6. Yogev S, Cooper R, Fetter R, Horowitz M, Shen K. Microtubule Organization Determines Axonal
506 Transport Dynamics. Neuron. 2016;92(2):449-60.
507 7. Bowne-Anderson H, Hibbel A, Howard J. Regulation of Microtubule Growth and Catastrophe:
508 Unifying Theory and Experiment. Trends in cell biology. 2015;25(12):769-79.
509 8. Rossi G, Redaelli V, Contiero P, Fabiano S, Tagliabue G, Perego P, et al. Tau Mutations Serve as a
510 Novel Risk Factor for Cancer. Cancer research. 2018;78(13):3731-9.
511 9. Tararuk T, Ostman N, Li W, Bjorkblom B, Padzik A, Zdrojewska J, et al. JNK1 phosphorylation of
512 SCG10 determines microtubule dynamics and axodendritic length. J Cell Biol. 2006;173(2):265-77.
513 10. Wen HL, Lin YT, Ting CH, Lin-Chao S, Li H, Hsieh-Li HM. Stathmin, a microtubule-destabilizing
514 protein, is dysregulated in spinal muscular atrophy. Human molecular genetics. 2010;19(9):1766-78.
515 11. Strang KH, Golde TE, Giasson BI. MAPT mutations, tauopathy, and mechanisms of
516 neurodegeneration. Laboratory investigation; a journal of technical methods and pathology.
517 2019;99(7):912-28.
518 12. Graf ER, Heerssen HM, Wright CM, Davis GW, DiAntonio A. Stathmin is required for stability of
519 the Drosophila neuromuscular junction. J Neurosci. 2011;31(42):15026-34.
520 13. Duncan JE, Lytle NK, Zuniga A, Goldstein LS. The Microtubule Regulatory Protein Stathmin Is
521 Required to Maintain the Integrity of Axonal Microtubules in Drosophila. PloS one. 2013;8(6):e68324.
522 14. Liedtke W, Leman EE, Fyffe RE, Raine CS, Schubart UK. Stathmin-deficient mice develop an age-
523 dependent axonopathy of the central and peripheral nervous systems. The American journal of
524 pathology. 2002;160(2):469-80.
525 15. Klim JR, Williams LA, Limone F, Guerra San Juan I, Davis-Dusenbery BN, Mordes DA, et al. ALS-
526 implicated protein TDP-43 sustains levels of STMN2, a mediator of motor neuron growth and repair. Nat
527 Neurosci. 2019;22(2):167-79.
528 16. Xiong Y, Zhao K, Wu J, Xu Z, Jin S, Zhang YQ. HDAC6 mutations rescue human tau-induced
529 microtubule defects in Drosophila. Proc Natl Acad Sci U S A. 2013;110(12):4604-9.
530 17. Braak H, Braak E. Neuropathological stageing of Alzheimer-related changes. Acta
531 neuropathologica. 1991;82(4):239-59.
532 18. Wittmann CW, Wszolek MF, Shulman JM, Salvaterra PM, Lewis J, Hutton M, et al. Tauopathy in
533 Drosophila: neurodegeneration without neurofibrillary tangles. Science. 2001;293(5530):711-4.
534 19. Mosavi LK, Cammett TJ, Desrosiers DC, Peng ZY. The ankyrin repeat as molecular architecture for
535 protein recognition. Protein science : a publication of the Protein Society. 2004;13(6):1435-48.
536 20. Sidor CM, Brain R, Thompson BJ. Mask proteins are cofactors of Yorkie/YAP in the Hippo
537 pathway. Current biology : CB. 2013;23(3):223-8.

538 21. Sansores-Garcia L, Atkins M, Moya IM, Shahmoradgoli M, Tao C, Mills GB, et al. Mask is required
539 for the activity of the Hippo pathway effector Yki/YAP. Current biology : CB. 2013;23(3):229-35.
540 22. Musco G, Kharrat A, Stier G, Fraternali F, Gibson TJ, Nilges M, et al. The solution structure of the
541 first KH domain of FMR1, the protein responsible for the fragile X syndrome. Nature structural biology.
542 1997;4(9):712-6.
543 23. Garcia-Mayoral MF, Hollingworth D, Masino L, Diaz-Moreno I, Kelly G, Gherzi R, et al. The
544 structure of the C-terminal KH domains of KSRP reveals a noncanonical motif important for mRNA
545 degradation. Structure (London, England : 1993). 2007;15(4):485-98.
546 24. Grishin NV. KH domain: one motif, two folds. Nucleic acids research. 2001;29(3):638-43.
547 25. Smith RK, Carroll PM, Allard JD, Simon MA. MASK, a large ankyrin repeat and KH domain-
548 containing protein involved in Drosophila receptor tyrosine kinase signaling. Development (Cambridge,
549 England). 2002;129(1):71-82.
550 26. Kallappagoudar S, Varma P, Pathak RU, Senthilkumar R, Mishra RK. Nuclear matrix proteome
551 analysis of Drosophila melanogaster. Mol Cell Proteomics. 2010;9(9):2005-18.
552 27. Müller H, Schmidt D, Steinbrink S, Mirgorodskaya E, Lehmann V, Habermann K, et al. Proteomic
553 and functional analysis of the mitotic Drosophila centrosome. The EMBO journal. 2010;29(19):3344-57.
554 28. Traina F, Favaro PM, Medina Sde S, Duarte Ada S, Winnischofer SM, Costa FF, et al. ANKHD1,
555 ankyrin repeat and KH domain containing 1, is overexpressed in acute leukemias and is associated with
556 SHP2 in K562 cells. Biochimica et biophysica acta. 2006;1762(9):828-34.
557 29. Dhyani A, Duarte AS, Machado-Neto JA, Favaro P, Ortega MM, Olalla Saad ST. ANKHD1 regulates
558 cell cycle progression and proliferation in multiple myeloma cells. FEBS letters. 2012;586(24):4311-8.
559 30. Machado-Neto JA, Lazarini M, Favaro P, Franchi GC, Jr., Nowill AE, Saad ST, et al. ANKHD1, a
560 novel component of the Hippo signaling pathway, promotes YAP1 activation and cell cycle progression in
561 prostate cancer cells. Experimental cell research. 2014;324(2):137-45.
562 31. Dhyani A, Machado-Neto JA, Favaro P, Saad ST. ANKHD1 represses p21 (WAF1/CIP1) promoter
563 and promotes multiple myeloma cell growth. European journal of cancer (Oxford, England : 1990).
564 2015;51(2):252-9.
565 32. Machado-Neto JA, Lazarini M, Favaro P, de Melo Campos P, Scopim-Ribeiro R, Franchi Junior GC,
566 et al. ANKHD1 silencing inhibits Stathmin 1 activity, cell proliferation and migration of leukemia cells.
567 Biochimica et biophysica acta. 2015;1853(3):583-93.
568 33. Zhu M, Li X, Tian X, Wu C. Mask loss-of-function rescues mitochondrial impairment and muscle
569 degeneration of Drosophila pink1 and parkin mutants. Human molecular genetics. 2015;24(11):3272-85.
570 34. Zhu M, Zhang S, Tian X, Wu C. Mask mitigates MAPT- and FUS-induced degeneration by
571 enhancing autophagy through lysosomal acidification. Autophagy. 2017;13(11):1924-38.
572 35. Zhu M, Zhang S, Tian X, Wu C. Mask mitigates MAPT- and FUS-induced degeneration by
573 enhancing autophagy through lysosomal acidification. Autophagy. 2017:1-15.
574 36. Chou VT, Johnson S, Long J, Vounatsos M, Van Vactor D. dTACC restricts bouton addition and
575 regulates microtubule organization at the Drosophila neuromuscular junction. Cytoskeleton (Hoboken,
576 NJ). 2020;77(1-2):4-15.
577 37. Akhmanova A, Steinmetz MO. Control of microtubule organization and dynamics: two ends in
578 the limelight. Nature reviews Molecular cell biology. 2015;16(12):711-26.
579 38. Hollingworth D, Candel AM, Nicastro G, Martin SR, Briata P, Gherzi R, et al. KH domains with
580 impaired nucleic acid binding as a tool for functional analysis. Nucleic acids research. 2012;40(14):6873-
581 86.
582 39. Karpova N, Bobinnec Y, Fouix S, Huitorel P, Debec A. Jupiter, a new Drosophila protein
583 associated with microtubules. Cell motility and the cytoskeleton. 2006;63(5):301-12.

584 40. Shi Q, Lin YQ, Saliba A, Xie J, Neely GG, Banerjee S. Tubulin Polymerization Promoting Protein,
585 Ringmaker, and MAP1B Homolog Futsch Coordinate Microtubule Organization and Synaptic Growth.
586 Frontiers in cellular neuroscience. 2019;13:192-.
587 41. Mitchison T, Kirschner M. Dynamic instability of microtubule growth. Nature.
588 1984;312(5991):237-42.
589 42. Chauvin S, Sobel A. Neuronal stathmins: a family of phosphoproteins cooperating for neuronal
590 development, plasticity and regeneration. Progress in neurobiology. 2015;126:1-18.
591 43. Stephan R, Goellner B, Moreno E, Frank CA, Hugenschmidt T, Genoud C, et al. Hierarchical
592 Microtubule Organization Controls Axon Caliber and Transport and Determines Synaptic Structure and
593 Stability. Developmental cell. 2015;33(1):5-21.
594 44. Brooks AN, Duff MO, May G, Yang L, Bolisetty M, Landolin J, et al. Regulation of alternative
595 splicing in Drosophila by 56 RNA binding proteins. Genome research. 2015;25(11):1771-80.
596 45. Tian X, Wu C. The role of ubiquitin-mediated pathways in regulating synaptic development,
597 axonal degeneration and regeneration: insights from fly and worm. The Journal of physiology.
598 2013;591(Pt 13):3133-43.
599 46. Keshishian H, Kim YS. Orchestrating development and function: retrograde BMP signaling in the
600 Drosophila nervous system. Trends Neurosci. 2004;27(3):143-7.
601 47. Bayat V, Jaiswal M, Bellen HJ. The BMP signaling pathway at the Drosophila neuromuscular
602 junction and its links to neurodegenerative diseases. Curr Opin Neurobiol. 2011;21(1):182-8.
603 48. Koles K, Budnik V. Wnt signaling in neuromuscular junction development. Cold Spring Harbor
604 perspectives in biology. 2012;4(6).
605 49. Franco B, Bogdanik L, Bobinnec Y, Debec A, Bockaert J, Parmentier ML, et al. Shaggy, the
606 homolog of glycogen synthase kinase 3, controls neuromuscular junction growth in Drosophila. The
607 Journal of neuroscience : the official journal of the Society for Neuroscience. 2004;24(29):6573-7.
608 50. Nechipurenko IV, Broihier HT. FoxO limits microtubule stability and is itself negatively regulated
609 by microtubule disruption. The Journal of cell biology. 2012;196(3):345-62.
610 51. Takeda M, Sami MM, Wang YC. A homeostatic apical microtubule network shortens cells for
611 epithelial folding via a basal polarity shift. Nature cell biology. 2018;20(1):36-45.
612 52. Chabu C, Doe CQ. Dap160/intersectin binds and activates aPKC to regulate cell polarity and cell
613 cycle progression. Development. 2008;135(16):2739.
614 53. Budnik V, Koh YH, Guan B, Hartmann B, Hough C, Woods D, et al. Regulation of synapse
615 structure and function by the Drosophila tumor suppressor gene dlg. Neuron. 1996;17(4):627-40.
616 54. Daniels RW, Collins CA, Gelfand MV, Dant J, Brooks ES, Krantz DE, et al. Increased expression of
617 the Drosophila vesicular glutamate transporter leads to excess glutamate release and a compensatory
618 decrease in quantal content. J Neurosci. 2004;24(46):10466-74.

619

620

621 **Figure Legends**

622 **Figure 1, *mask* negatively regulates microtubule stability in larval muscle and enhances**
623 **Tau-induced MT fragmentation.**

624 (**A**) Representative confocal images of microtubule (MT) in muscle 6 of wild type, *mask* null
625 ($mask^{10.22/Df}$), rescue of *mask* null with a 24B (muscle-specific)-Gal4-driven UAS-Mask
626 transgene, 24B -Gal4-driven UAS-Vector, UAS-*mask* RNAi, or UAS-Mask.. MTs are
627 immunostained with an anti-Acetylated Tubulin antibody. Yellow dash lines denote the edge of
628 muscle nuclei. Scale bar: 5 µm. (**B**) Quantification of average MT lengths. (**C**) Representative
629 confocal images of MT in muscle 6 of 24B-Gal4/+, 24B-Gal4-driven UAS-human Tau (hTau)
630 with UAS-Td-Tomato, UAS-*mask* RNAi, or UAS-Mask. MTs are immunostained with an anti-
631 Acetylated Tubulin antibody. Scale bar: 5 µm. (**D**) Quantification of average MT lengths.

632 **Figure 2, *mask* knockdown increase formation of longer MTs in fly larval muscles.**

633 (**A**) Western analysis of total proteins and ultracentrifugal fractions (supernatant and pellet) in
634 larval muscle lysates from wild type control or *mask* knockdown (24B-Gal4-driven *mask* RNAi).
635 Lysates were treated with either 100 µm or 100 nm Taxol. Anti-beta-Tubulin and anti-alpha-
636 Actin blots were performed on total and ultracentrifugal fractions of both lysates. (**B**)
637 Quantification of the relative levels of Tubulin fractionated in the pellet fraction in the lysate
638 treated by 100 nm Taxol. The levels of Tubulin in pellet were normalized to the levels of total
639 Tubulin. n = 3 trials.

640

641 **Figure 3, Mask promotes normal NMJ terminal growth by regulating motor neuron**
642 **microtubule stability.**

643 (**A**) Representative confocal images of larval muscle 4 NMJs in wild type, *mask* null
644 (*mask*$^{10.22/Df}$), *mask* null rescued with a UAS-Mask transgene driven by pan-neuron (BG380),
645 ubiquitous (DA) or muscle (MHC) Gal4 drivers, and *stathmin*/*mask* double mutant (*stai*$^{B200/L27}$;
646 *mask*$^{10.22/Df}$). Scale bar: 10 µm. (**B**) Quantification of the number of boutons, synaptic span and
647 the number of branching points at the Muscle 4 NMJs. Each data point was normalized to the
648 size of the imaged muscle 4. (**C**) Representative confocal images of native GFP fluorescence
649 plus a very brief staining of Cy3-HRP (see method section) of segmental nerves in 3rd instar
650 larvae containing Elav-driven UAS-EB1-GFP with UAS-vector or with UAS-*mask* RNAi. Scale
651 bar: 20 µm. (**D**) Quantification of average number of EB1-GFP comets normalized to nerve
652 area.

653 **Figure 4, *mask* and *stai* reciprocally suppress each other.** (**A, B**) Loss of *stai* function
654 suppresses the synaptic terminal over-expansion caused by *mask* loss-of-function in a dose-
655 dependent manner. (**A**) Representative confocal images of muscle 4 NMJs in larvae with Elav-
656 driven UAS-vector, Elav-driven UAS-*mask* RNAi in wild type background, *stai* heterozygous
657 (*stai*$^{B200/+}$) or *stai* homozygous (*stai*$^{B200/L27}$)mutant backgrounds. Scale bar, 10 µm. (**B**)
658 quantification of the number of boutons, synaptic span and the number of branching points at the
659 muscle 4 NMJs. Each data point was normalized to the size of the imaged muscle 4. NMJs were
660 immunostained with anti-HRP (red) and anti-DVGlut (green) antibodies. (**C, D, E**) Loss of *mask*
661 function in neurons suppresses *stai* mutant defects in NMJ development and axonal transport**.**
662 (**C, D**) Representative confocal images of muscle 4 NMJs (C) and lateral nerve bundles (D) in

663 wild type, *stai* (*stai*$^{B200/L27}$), *stai*/*mask* double mutant (*stai*$^{B200/L27}$;*mask*$^{10.22/Df}$), or *stai* mutant with
664 pan-neuronal expression of *mask* RNAi. Larval NMJs were immunostained with anti-DVGlut
665 (green), anti-DLG (red), and anti-HRP (blue). Arrows point to synaptic boutons that have
666 postsynaptic DLG staining but lack presynaptic DVGLut staining (so-called footprint). Brackets
667 highlight the lateral axons that shows residual DVGlut staining. Scale bars, 10 µm for C; 5 µm
668 for D. (**E**) Quantification of the number of foot-printing boutons in muscle 4 NMJs at segment
669 A3 and A4, as well as axonal accumulation of DVGlut.

670 **Figure 5, Rescue experiments identify structural requirement for Mask's action in**
671 **regulating MT stability.**

672 (**A**) A schematic of wild type and mutant UAS-Mask transgenes used in the rescue experiments
673 and the representative western blots showing muscle expression of endogenous Mask in wild
674 type or each of the four UAS-Mask transgenes expressed in muscles in *mask* null mutants. Note
675 that the anti-Mask antibody does not recognize GFP-Mask-KH-Only protein, indicating the
676 antigen of this antibody is outside of the Mask-KH-Only region. Anti-GFP western blots were
677 performed to show the expression of GFP-Mask-KH-Only (indicated by an asterisk). (**B**)
678 Representative confocal images of MT in muscle 6 of wild type, *mask* null (*mask*$^{10.22/Df}$), and
679 rescues of *mask* null with MHC-Gal4-driven UAS-Mask, UAS-Mask-KH-Mut, UAS-Mask-KH-
680 Only, or UAS-Mask-ANK transgenes. MTs are immunostained with an anti-Acetylated Tubulin
681 antibody. Scale bar: 10 µm. (**C**) Quantification of average MT lengths. (**D**) Representative
682 confocal images of muscle 4 NMJs in wild type, *mask* null (*mask*$^{10.22/Df}$), rescues of *mask* null
683 with pan-neuron (BG380) driven wild type or mutant/deletion UAS-Mask transgenes as shown
684 in A. Scale bar: 10 µm. (**E**) quantification of the number of boutons, synaptic span and the

685 number of branching points at the muscle 4 NMJs. Each data point was normalized to the size of
686 the imaged muscle 4.

687 **Figure 6, Mask genetically interacts with Jupiter and regulates its localization to**
688 **microtubules.**

689 **(A, C)** Representative confocal images of segmental nerves (A), or muscle 4 NMJs (C), immune-
690 stained with anti-mCherry (Red) and anti-Futsch (green) antibodies in 3rd instar larvae of flies
691 expressing Elav-driven UAS-mCherry-Jupiter together with UAS-control RNAi, UAS-*mask*
692 RNAi or UAS-Mask. (**B, D**) Quantification of the mean intensity of mCherry and Futsch. (**E**)
693 Representative confocal images of muscle 4 NMJs in wild type, *mask* null ($mask^{10.22/Df}$), Elav-
694 driven *Jupiter* RNAi (VDRC: KK116151), and BG380-driven *Jupiter* RNAi in the *mask* null
695 mutants. (**F**) Quantification of the number of boutons, synaptic span and the number of
696 branching points at the muscle 4 NMJs. Each data point was normalized to the size of the muscle
697 4 that were imaged. Scale bars: 10 µm.

Figure S1

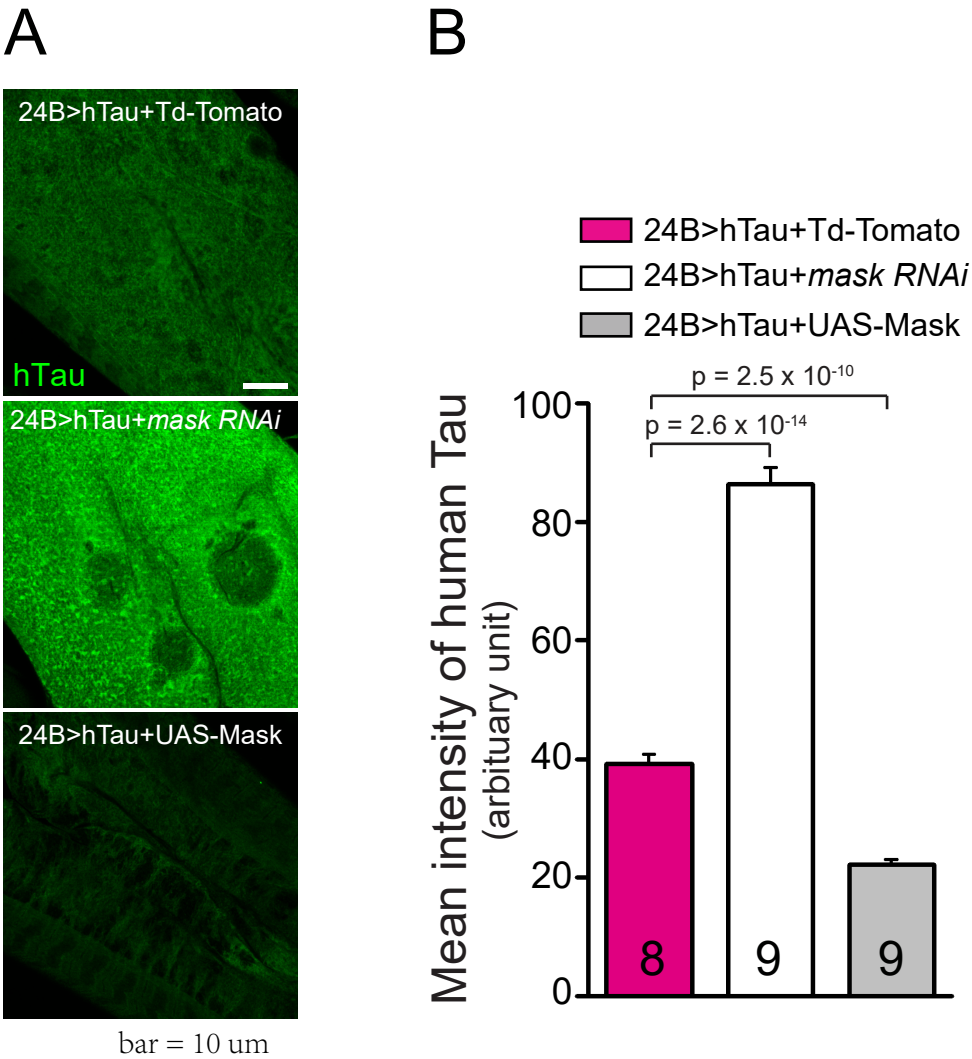
A
24B>hTau+Td-Tomato
hTau
24B>hTau+mask RNAi
24B>hTau+UAS-Mask
bar = 10 um
B
24B>hTau+Td-Tomato
24B>hTau+mask RNAi
24B>hTau+UAS-Mask
p = 2.5 x 10-10
p = 2.6 x 10-14
Mean intensity of human Tau
(arbituary unit)
100
80
60
40
20
0
8
9
9

Figure S2

A

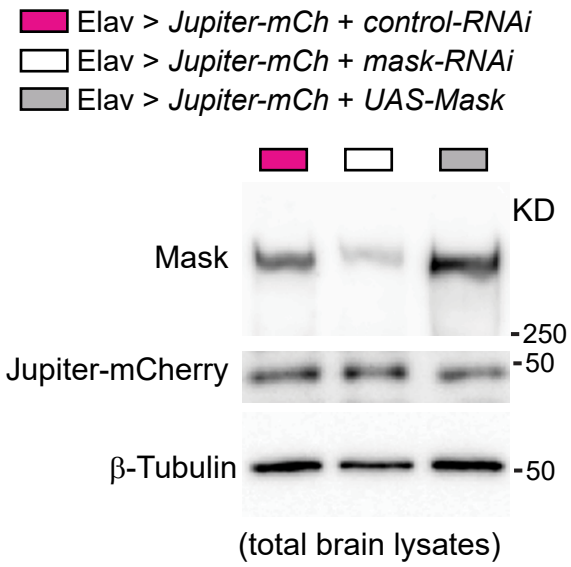
Elav > *Jupiter-mCh* + *control-RNAi*
Elav > *Jupiter-mCh* + *mask-RNAi*
Elav > *Jupiter-mCh* + *UAS-Mask*
KD
Mask
-250
Jupiter-mCherry
-50
β-Tubulin
-50
(total brain lysates)

B

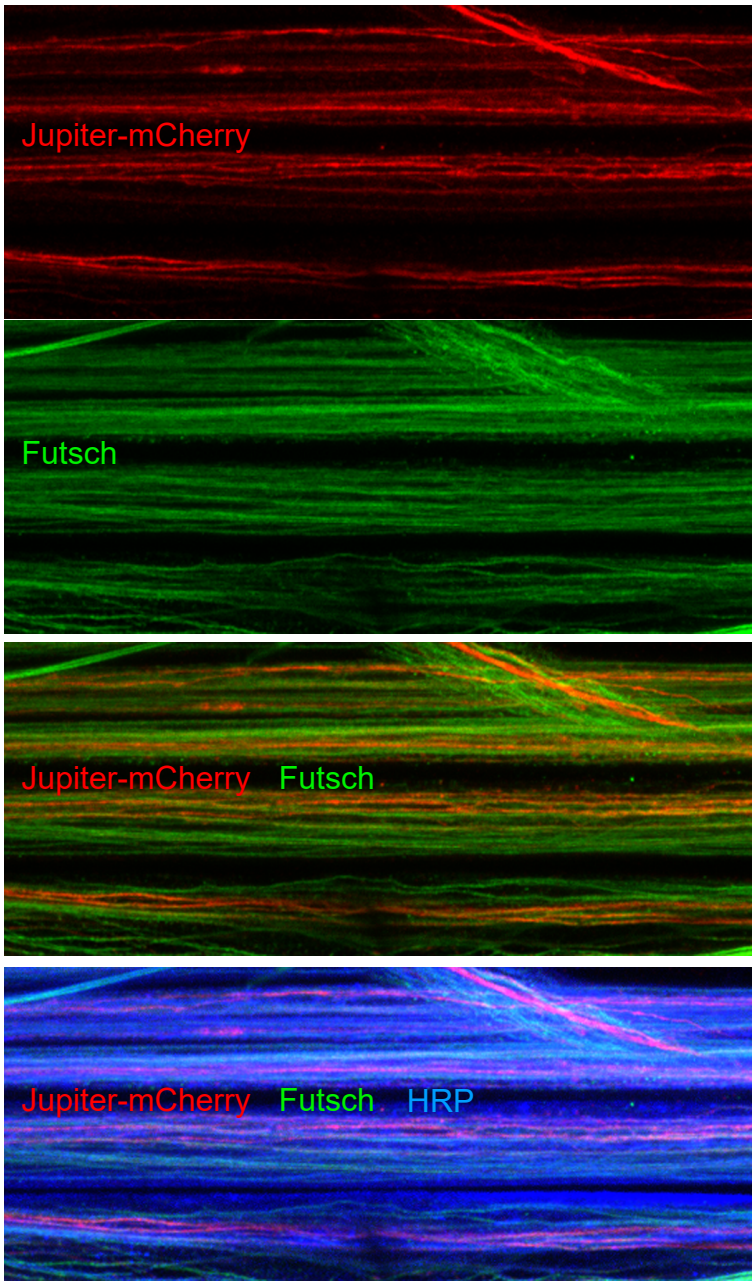
Jupiter-mCherry
Futsch
Jupiter-mCherry Futsch
Jupiter-mCherry Futsch HRP

Figure S3

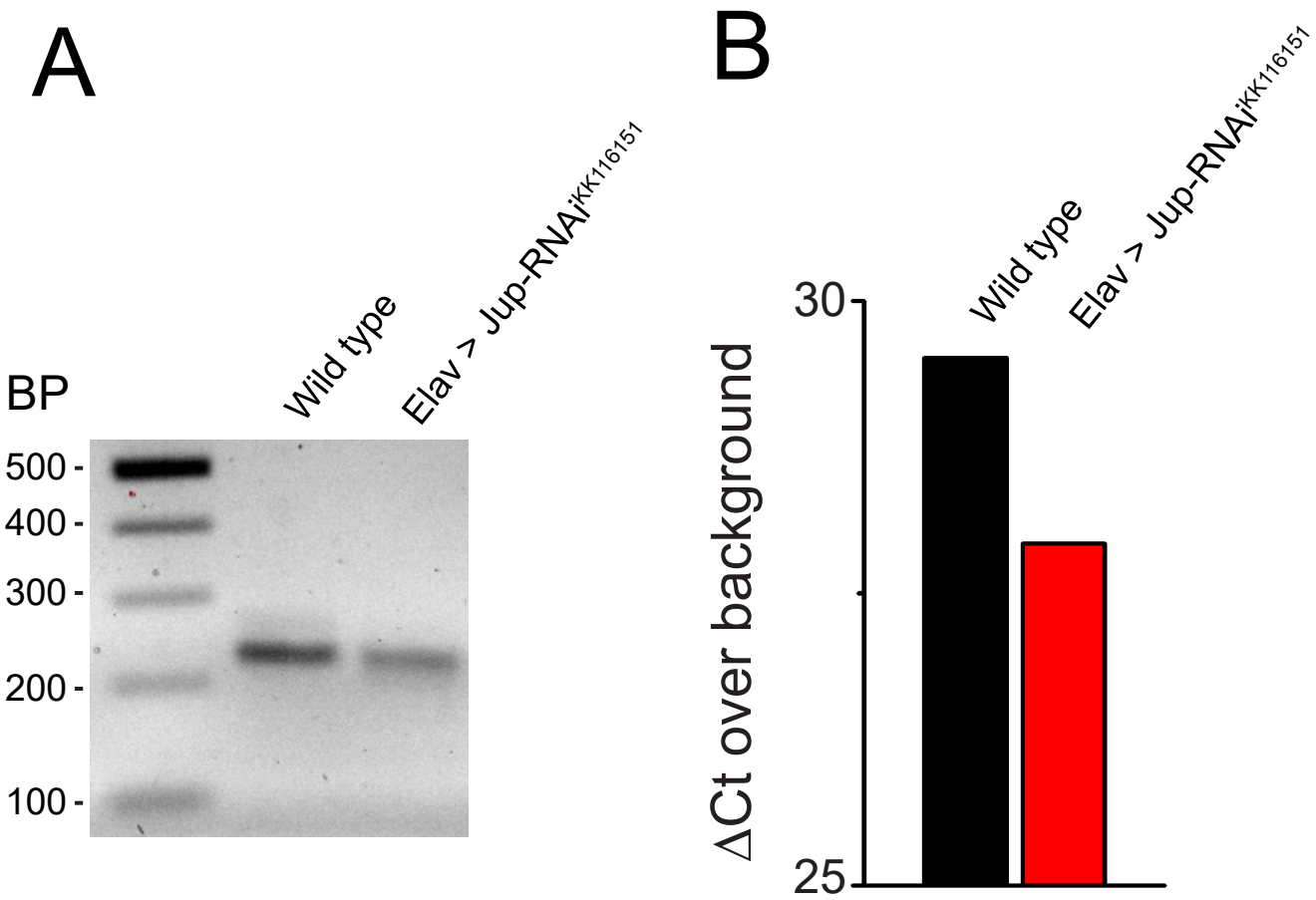
A
BP
500
400
300
200
100
Wild type
Elav > Jup-RNAi iKK116151
B
30
25
ΔCt over background
Wild type
Elav > Jup-RNAi iKK116151

Supplemental Figure 1, Mask regulates the abundance of Tau protein in larval muscles.

(**A**) Representative confocal images of hTau expression in muscle 6 of 24B-Gal4-driven UAS-human Tau (hTau) together with UAS-Td-Tomato, UAS-*mask* RNAi, or UAS-Mask. Human Tau proteins were immunostained with an anti-Tau antibody. Scale bar: 10 µm. (**B**) Quantification of the mean intensity of hTau in the larval muscles.

Supplemental Figure 2, Up- or down-regulation of Mask in fly brains does not change the levels of Jupiter-mCherry expression, and Jupiter-mCherry and Futsch show preferential association to distinct pools of MTs.

(**A**) Western blot analysis of larval brains expressing Jupiter-mCherry together with UAS-control-RNAi, UAS-*mask*-RNAi, or UAS-Mask with anti-Mask, anti-mCherry, and anti-β-Tubulin antibodies. (**B**) Representative confocal images of segmental nerves of 3rd instar larvae of Elav-driven Jupiter-mCherry and UAS-*mask*-RNAi. Notice the largely non-overlapping pattern of Jupiter-mCherry and Futsch. Scale bar: 10 µm.

Supplemental Figure 3, neuronal expression of Jup-RNAi line KK116151 effectively knocks down Jupiter mRNA levels.

(**A**) A representative conventional RT-PCR result showing a ~230-bp *Jupiter* PCR fragment amplified from wild type larval brains or brains expressing *UAS-Jup-RNAi*^{KK116151} (driven by elav-Gal4). (**B**) Quantitative RT-PCR shows reduction of Jupiter mRNA to ~33% (2^-ΔΔCt) compared to wild type control. The transcript of RPL32was used as the internal control (reference gene) to calculate the ΔCt in control and RNAi samples. Note that the y axis values are expressed as log2 values relative to levels in wells containing no cDNA ("backbround"=Ct

40) following RPL32 normalization; hence, zero indicates essentially no detectable levels of given amplicon and higher numbers = higher amounts of starting RNA.

Figure 1

A

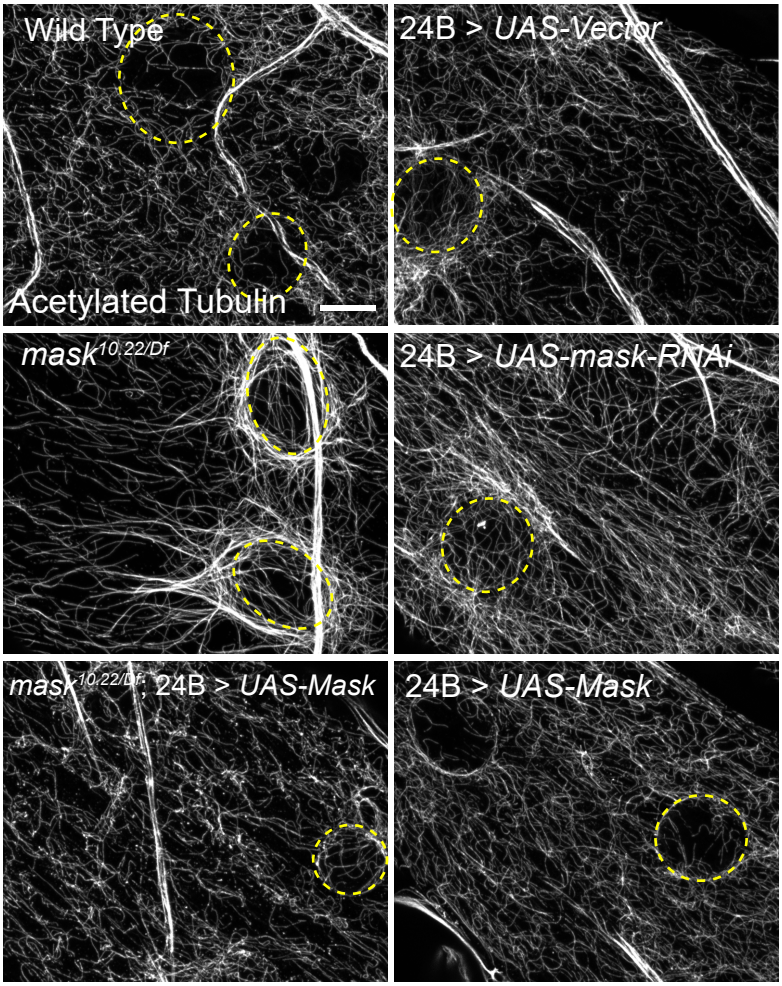

B

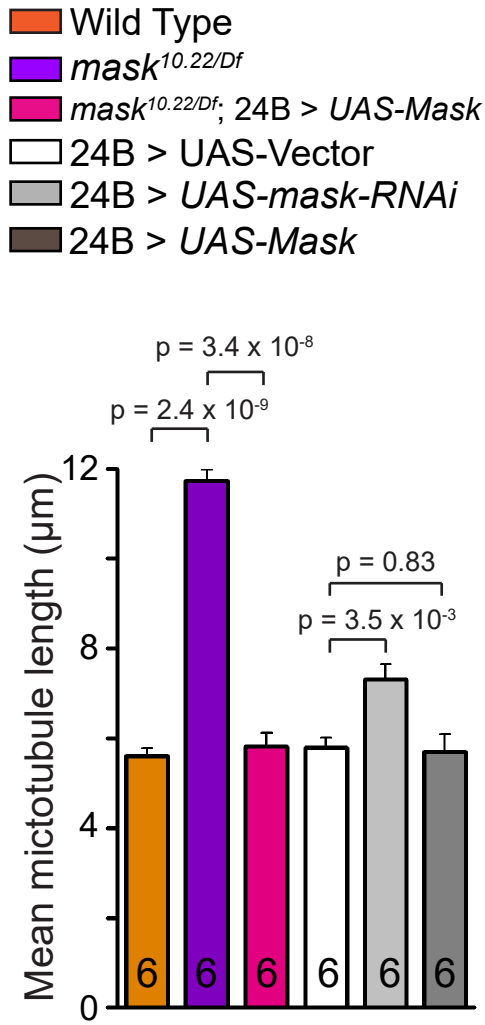

C

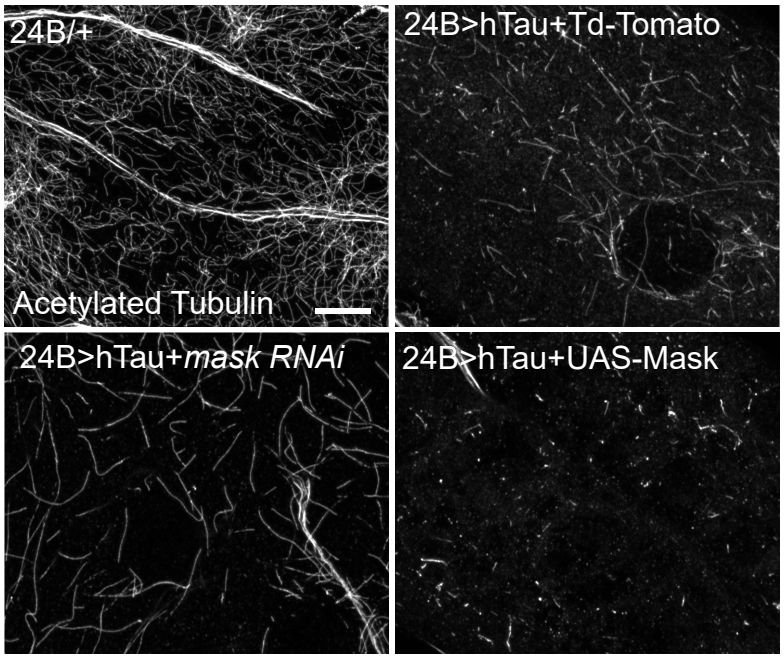

D

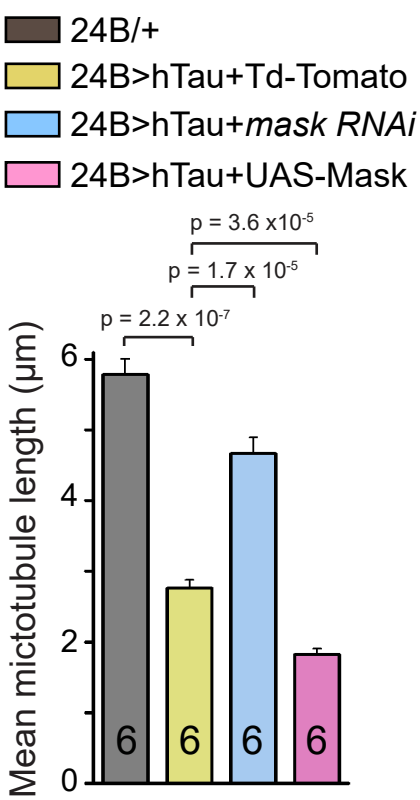

Figure 2

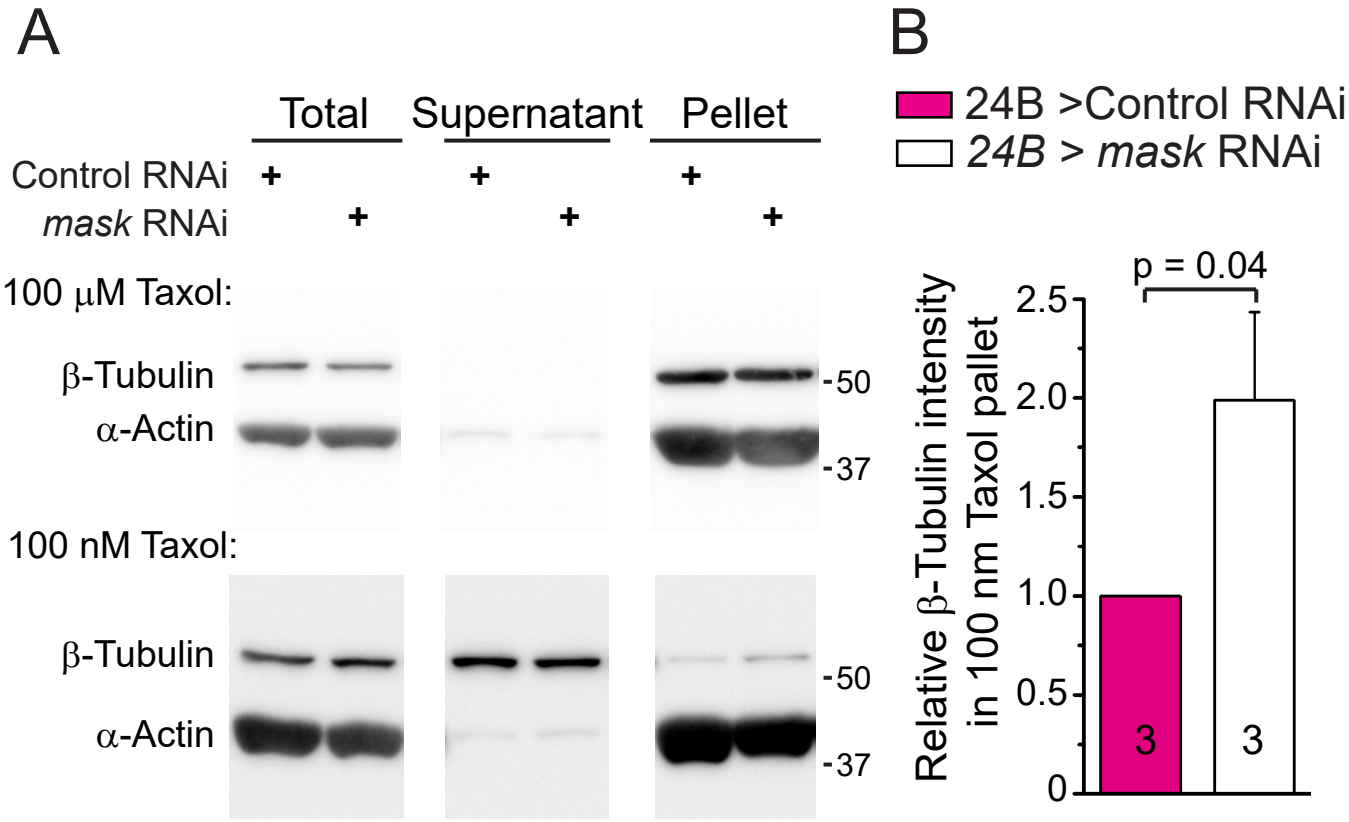
A
Total
Supernatant
Pellet
Control RNAi
mask RNAi
100 μM Taxol:
β-Tubulin
α-Actin
-50
-37
100 nM Taxol:
β-Tubulin
α-Actin
-50
-37
B
24B >Control RNAi
24B > mask RNAi
p = 0.04
Relative β-Tubulin intensity in 100 nm Taxol pallet
2.5
2.0
1.5
1.0
0.5
0
3
3

Figure 3

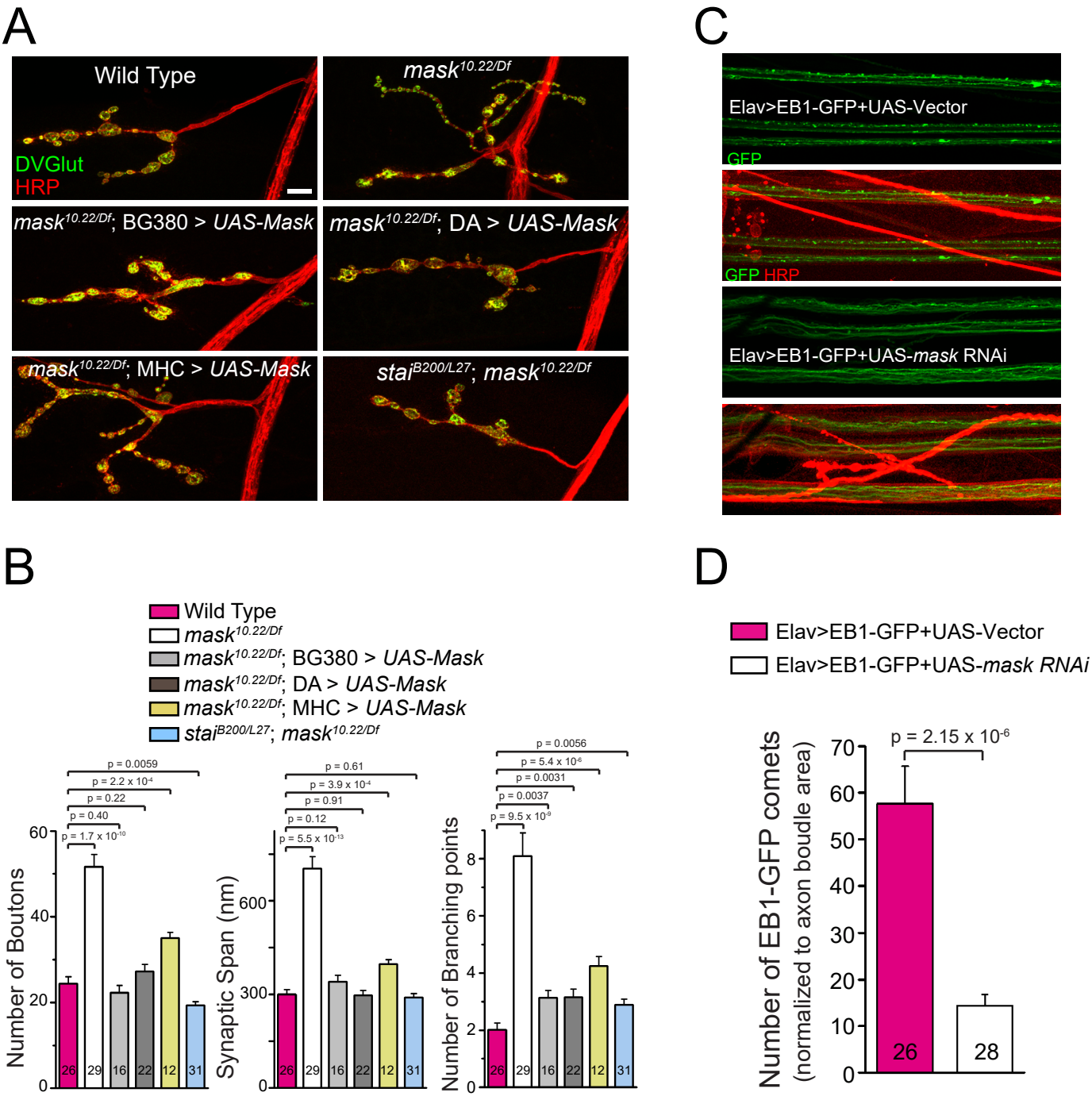
A
Wild Type
DVGlut
HRP
mask10.22/Df
mask10.22/Df; BG380 > UAS-Mask
mask10.22/Df; DA > UAS-Mask
mask10.22/Df; MHC > UAS-Mask
staiB200/L27; mask10.22/Df
C
Elav>EB1-GFP+UAS-Vector
GFP
GFP HRP
Elav>EB1-GFP+UAS-mask RNAi
B
Wild Type
mask10.22/Df
mask10.22/Df; BG380 > UAS-Mask
mask10.22/Df; DA > UAS-Mask
mask10.22/Df; MHC > UAS-Mask
staiB200/L27; mask10.22/Df
Number of Boutons
p = 0.0059
p = 2.2 x 10-4
p = 0.22
p = 0.40
p = 1.7 x 10-10
Synaptic Span (nm)
p = 0.61
p = 3.9 x 10-4
p = 0.91
p = 0.12
p = 5.5 x 10-13
Number of Branching points
p = 0.0056
p = 5.4 x 10-6
p = 0.0031
p = 0.0037
p = 9.5 x 10-9
26 29 16 22 12 31
D
Elav>EB1-GFP+UAS-Vector
Elav>EB1-GFP+UAS-mask RNAi
Number of EB1-GFP comets
(normalized to axon boudle area)
p = 2.15 x 10-6
26
28

Figure 4

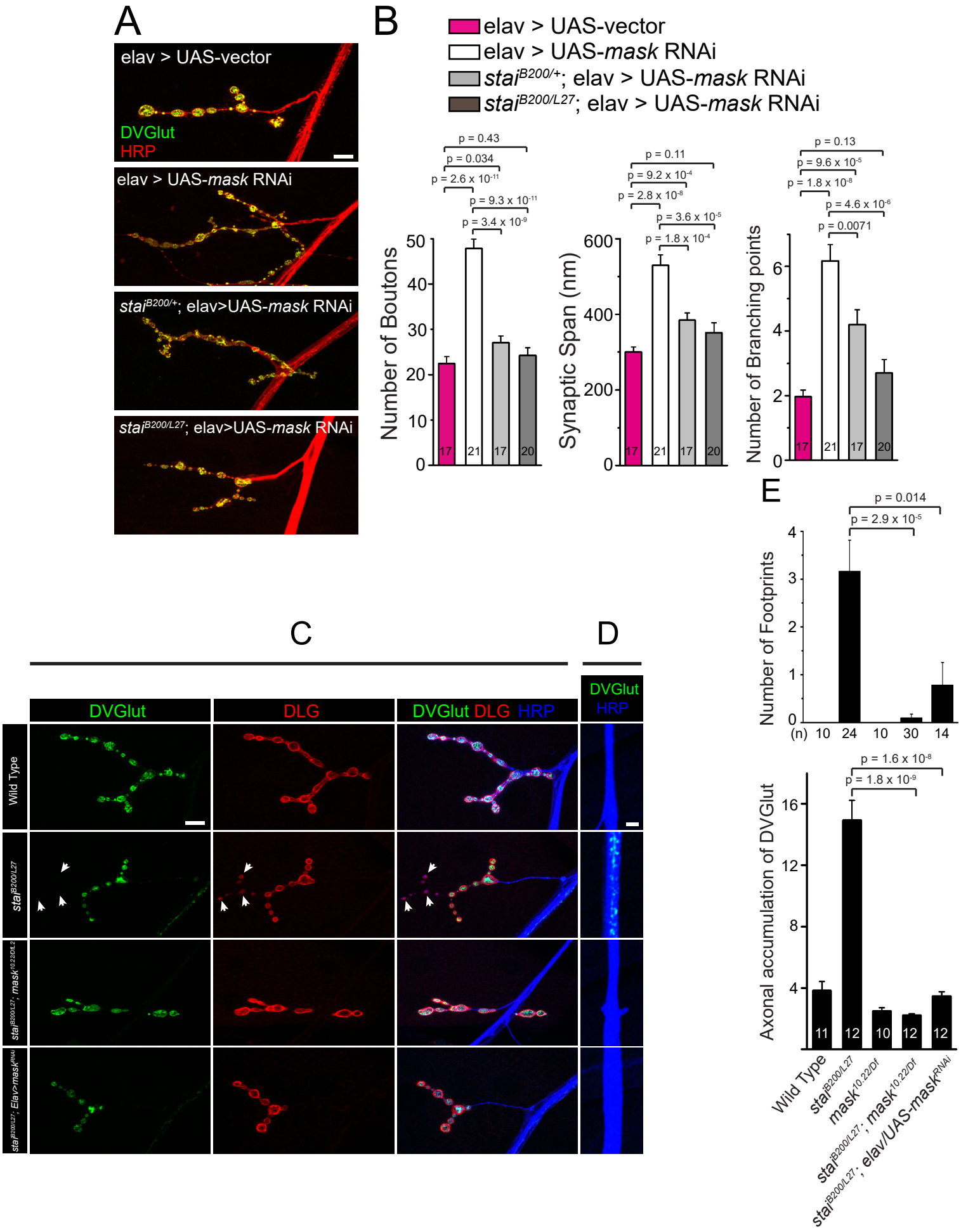
A
elav > UAS-vector
DVGlut
HRP
elav > UAS-mask RNAi
staiB200/+; elav>UAS-mask RNAi
staiB200/L27; elav>UAS-mask RNAi
B
elav > UAS-vector
elav > UAS-mask RNAi
staiB200/+; elav > UAS-mask RNAi
staiB200/L27; elav > UAS-mask RNAi
Number of Boutons
p = 0.43
p = 0.034
p = 2.6 x 10-11
p = 9.3 x 10-11
p = 3.4 x 10-9
Synaptic Span (nm)
p = 0.11
p = 9.2 x 10-4
p = 2.8 x 10-8
p = 3.6 x 10-5
p = 1.8 x 10-4
Number of Branching points
p = 0.13
p = 9.6 x 10-5
p = 1.8 x 10-8
p = 4.6 x 10-6
p = 0.0071
17
21
17
20
C
D
DVGlut
DLG
DVGlut DLG HRP
DVGlut
HRP
Wild Type
staiB200/L27
staiB200/L27; mask10.22/Df.2
staiB200/L27; Elav>maskRNAi
E
Number of Footprints
p = 0.014
p = 2.9 x 10-5
(n) 10 24 10 30 14
Axonal accumulation of DVGlut
p = 1.6 x 10-8
p = 1.8 x 10-9
11 12 10 12 12
Wild Type
staiB200/L27
mask10.22/Df
staiB200/L27; mask10.22/Df
staiB200/L27; elav/UAS-maskRNAi

Figure 5

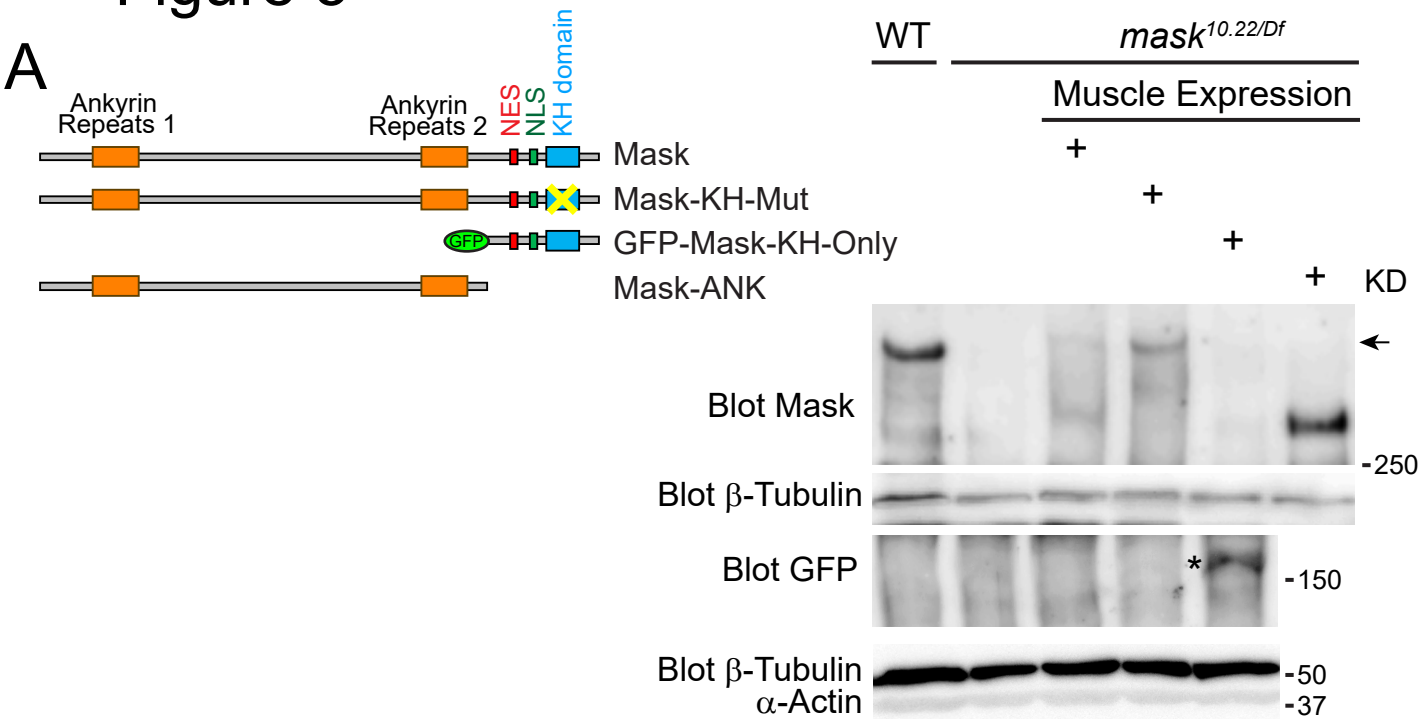
A
Ankyrin Repeats 1
Ankyrin Repeats 2
NES
NLS
KH domain
Mask
Mask-KH-Mut
GFP
GFP-Mask-KH-Only
Mask-ANK
WT
mask10.22/Df
Muscle Expression
KD
Blot Mask
Blot β-Tubulin
Blot GFP
Blot β-Tubulin
α-Actin
-250
-150
-50
-37

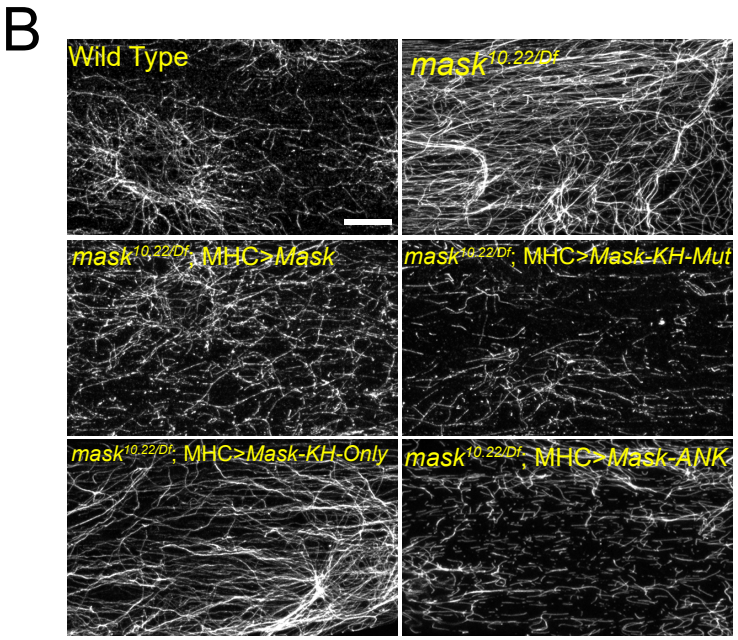
B
Wild Type
mask10.22/Df
mask10.22/Df; MHC>Mask
mask10.22/Df; MHC>Mask-KH-Mut
mask10.22/Df; MHC>Mask-KH-Only
mask10.22/Df; MHC>Mask-ANK

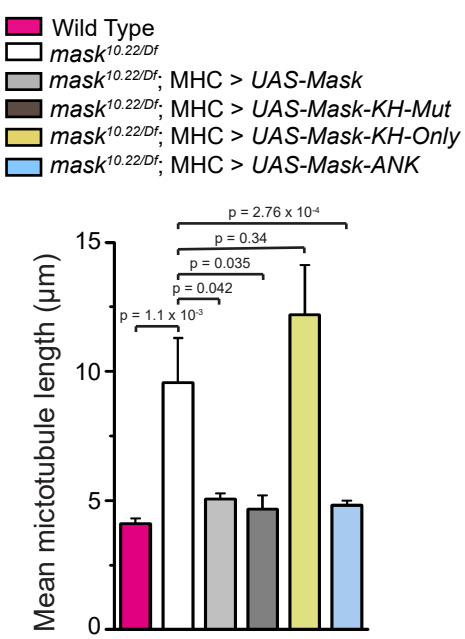
C
Wild Type
mask10.22/Df
mask10.22/Df; MHC > UAS-Mask
mask10.22/Df; MHC > UAS-Mask-KH-Mut
mask10.22/Df; MHC > UAS-Mask-KH-Only
mask10.22/Df; MHC > UAS-Mask-ANK
Mean mictotubule length (μm)
p = 2.76 x 10-4
p = 0.34
p = 0.035
p = 0.042
p = 1.1 x 10-3

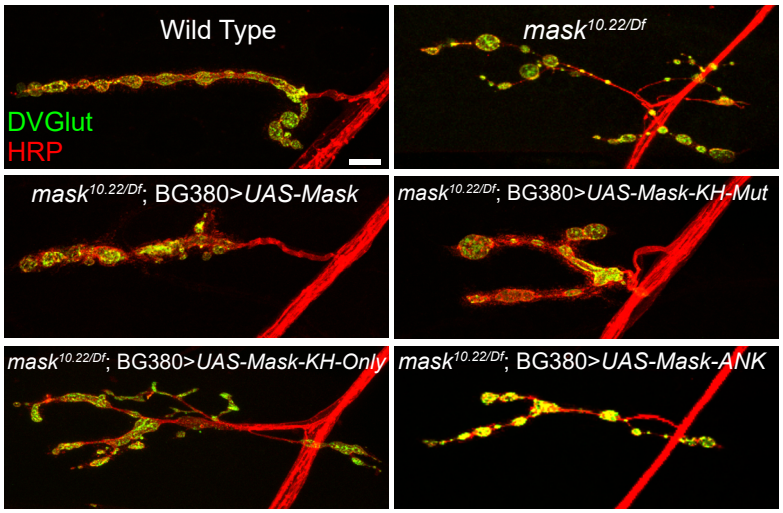
D
Wild Type
DVGlut
HRP
mask10.22/Df
mask10.22/Df; BG380>UAS-Mask
mask10.22/Df; BG380>UAS-Mask-KH-Mut
mask10.22/Df; BG380>UAS-Mask-KH-Only
mask10.22/Df; BG380>UAS-Mask-ANK

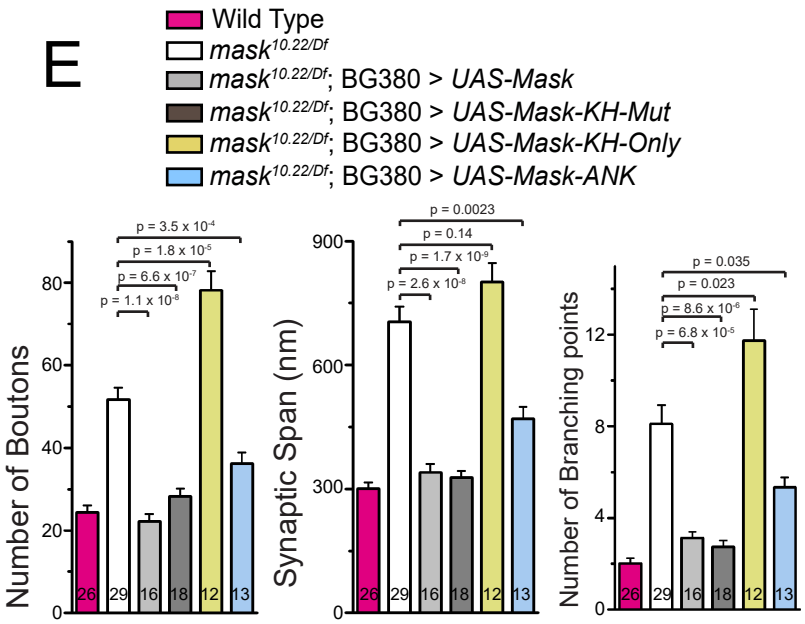
E
Wild Type
mask10.22/Df
mask10.22/Df; BG380 > UAS-Mask
mask10.22/Df; BG380 > UAS-Mask-KH-Mut
mask10.22/Df; BG380 > UAS-Mask-KH-Only
mask10.22/Df; BG380 > UAS-Mask-ANK
Number of Boutons
Synaptic Span (nm)
Number of Branching points
p = 3.5 x 10-4
p = 1.8 x 10-5
p = 6.6 x 10-7
p = 1.1 x 10-8
p = 0.0023
p = 0.14
p = 1.7 x 10-9
p = 2.6 x 10-8
p = 0.035
p = 0.023
p = 8.6 x 10-6
p = 6.8 x 10-5
26
29
16
18
12
13

Figure 6

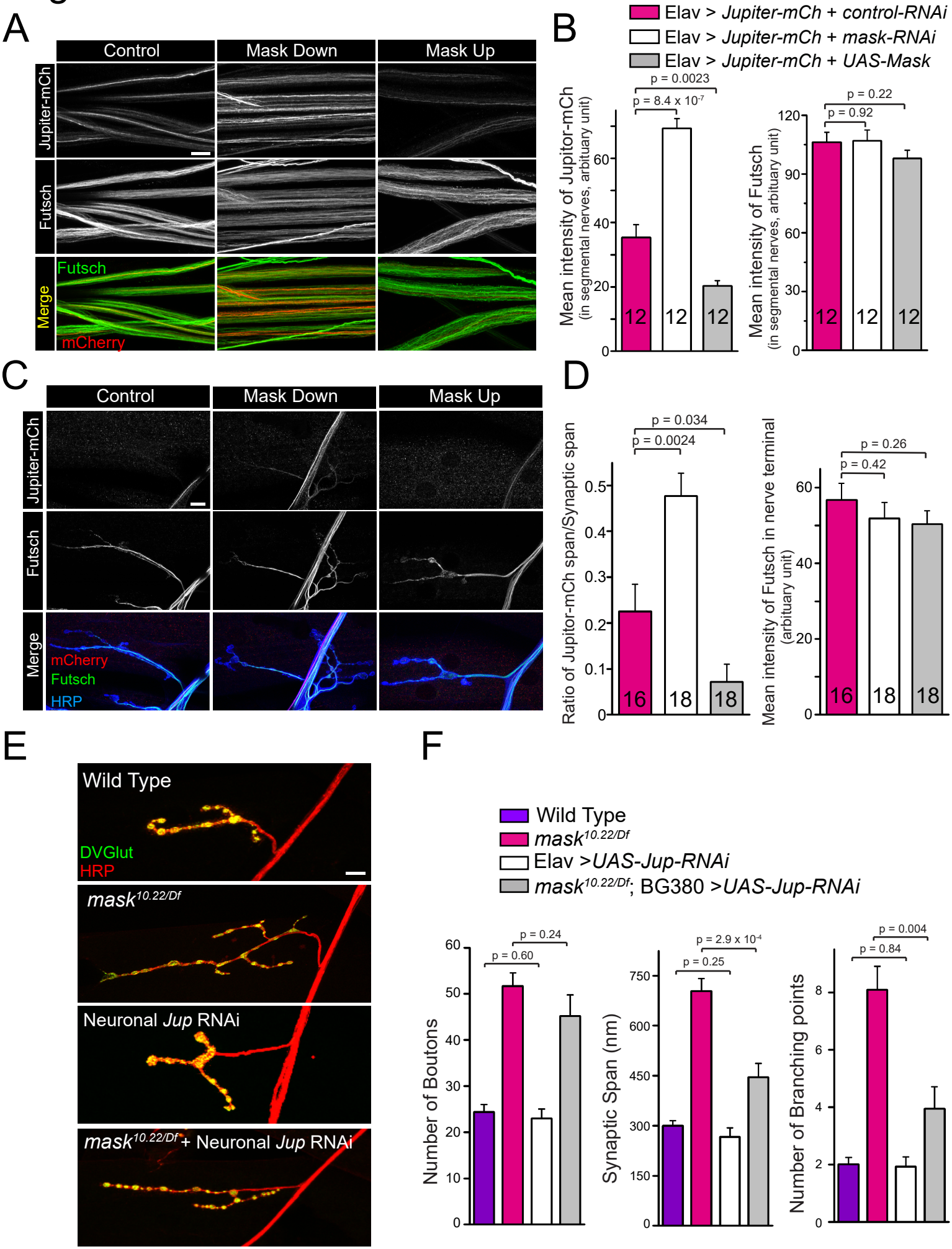
A
Control
Mask Down
Mask Up
Jupiter-mCh
Futsch
Merge
Futsch
mCherry
B
Elav > Jupiter-mCh + control-RNAi
Elav > Jupiter-mCh + mask-RNAi
Elav > Jupiter-mCh + UAS-Mask
Mean intensity of Jupitor-mCh
(in segmental nerves, arbituary unit)
p = 0.0023
p = 8.4 x 10-7
Mean intensity of Futsch
(in segmental nerves, arbituary unit)
p = 0.22
p = 0.92
12
12
12
C
Control
Mask Down
Mask Up
Jupiter-mCh
Futsch
Merge
mCherry
Futsch
HRP
D
Ratio of Jupitor-mCh span/Synaptic span
p = 0.034
p = 0.0024
Mean intensity of Futsch in nerve terminal
(arbituary unit)
p = 0.26
p = 0.42
16
18
18
E
Wild Type
DVGlut
HRP
mask10.22/Df
Neuronal Jup RNAi
mask10.22/Df + Neuronal Jup RNAi
F
Wild Type
mask10.22/Df
Elav >UAS-Jup-RNAi
mask10.22/Df; BG380 >UAS-Jup-RNAi
Number of Boutons
p = 0.24
p = 0.60
Synaptic Span (nm)
p = 2.9 x 10-4
p = 0.25
Number of Branching points
p = 0.004
p = 0.84